NAVAL POSTGRADUATE SCHOOL
Monterey, California

THESIS

INTEGRATED OPTICAL FIBER LATTICE ACCUMULATORS

by

Adam F. Atherton

March 1997

Thesis Advisor Phillip E. Pace

Approved for public release; distribution is unlimited.

REPORT DOCUMENTATION PAGE

Form Approved OMB No. 0704-0188

1. AGENCY USE ONLY *(Leave blank)*	2. REPORT DATE March 1997	3. REPORT TYPE AND DATES COVERED Master's Thesis

4. TITLE AND SUBTITLE TITLE OF THESIS Integrated Optical Fiber Lattice Accumulators

5. FUNDING NUMBERS

6. AUTHOR(S) Adam F. Atherton

7. PERFORMING ORGANIZATION NAME(S) AND ADDRESS(ES)
Naval Postgraduate School
Monterey CA 93943-5000

8. PERFORMING ORGANIZATION REPORT NUMBER

9. SPONSORING/MONITORING AGENCY NAME(S) AND ADDRESS(ES)
Space and Naval Warfare Systems Command

10. SPONSORING/MONITORING AGENCY REPORT NUMBER

11. SUPPLEMENTARY NOTES The views expressed in this thesis are those of the author and do not reflect the official policy or position of the Department of Defense or the U.S. Government.

12a. DISTRIBUTION/AVAILABILITY STATEMENT Approved for public release; distribution unlimited

12b. DISTRIBUTION CODE

13. ABSTRACT *(maximum 200 words)*

Sigma-delta modulators track a signal by accumulating the error between an input signal and a feedback signal. The accumulated energy is amplitude analyzed by a comparator. The comparator output signal is fed back and subtracted from the input signal. This thesis is primarily concerned with designing accumulators for inclusion in an optical sigma-delta modulator. Fiber lattice structures with optical amplifiers are used to perform the accumulation. Two fiber lattice structures are designed, modeled, tuned, tested, and characterized. The testing results for both models are plotted and tabulated. One result is that accumulation is inversely proportional to coupling ratio. Also, the optical gain necessary to drive either fiber lattice structure to a monotonically increasing response is identical. With less than 10 dB of optical gain, a wide range of accumulation rates are available. Initial integration of one fiber lattice structure into a first-order sigma-delta modulator is accomplished with results consistent with those from an ideal model. The design for a second-order sigma-delta modulator is developed, tested, and preliminary results shown.

14. SUBJECT TERMS ADC, Fiber Lattice Structures, Directional Coupler, Sigma Delta			15. NUMBER OF PAGES 76
			16. PRICE CODE
17. SECURITY CLASSIFICATION OF REPORT Unclassified	18. SECURITY CLASSIFICATION OF THIS PAGE Unclassified	19. SECURITY CLASSIFICATION OF ABSTRACT Unclassified	20. LIMITATION OF ABSTRACT UL

NSN 7540-01-280-5500

Standard Form 298 (Rev. 2-89)
Prescribed by ANSI Std. 239-18 298-102

Approved for public release; distribution is unlimited

INTEGRATED OPTICAL FIBER LATTICE ACCUMULATORS

Adam F. Atherton
Edwards AFB, CA
B.S., California State University, Fresno, Fresno, CA 1988

Submitted in partial fulfillment of the
requirements for the degree of

MASTER OF SCIENCE IN ELECTRICAL ENGINEERING

from the

NAVAL POSTGRADUATE SCHOOL

March 1997

Author: 

Adam F. Atherton

Approved by: 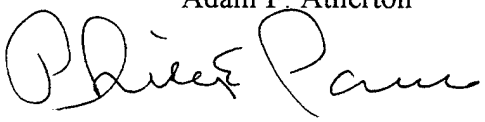

Phillip E. Pace, Thesis Advisor

John R. Powers, Second Reader

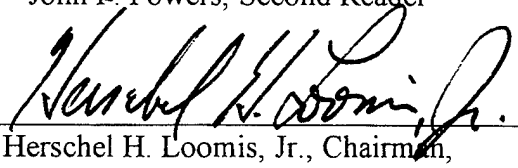

Herschel H. Loomis, Jr., Chairman,
Department of Electrical and Computer Engineering

ABSTRACT

Sigma-delta modulators track a signal by accumulating the error between an input signal and a feedback signal. The accumulated energy is amplitude analyzed by a comparator. The comparator output signal is fed back and subtracted from the input signal. This thesis is primarily concerned with designing accumulators for inclusion in an optical sigma-delta modulator. Fiber lattice structures with optical amplifiers are used to perform the accumulation. Two fiber lattice structures are designed, modeled, tuned, tested, and characterized. The testing results for both models are plotted and tabulated. One result is that accumulation is inversely proportional to coupling ratio. Also, the optical gain necessary to drive either fiber lattice structure to a monotonically increasing response is identical. With less than 10 dB of optical gain, a wide range of accumulation rates are available. Initial integration of one fiber lattice structure into a first-order sigma-delta modulator is accomplished with results consistent with those from an ideal model. The design for a second-order sigma-delta modulator is developed, tested, and preliminary results shown.

TABLE OF CONTENTS

LIST OF FIGURES

LIST OF TABLES

LIST OF SYMBOLS, ACRONYMS, AND/OR ABBREVIATIONS

κ	Coupling Coefficient
p	Extinction Coefficient
N	Effective Index
V	Fiber Parameter
δn	Index Difference
G	Optical Amplifier
$\Delta\beta L$	Phase Mismatch Parameter
ζ	Pockels Coefficient
β	Propagation Constant in Material
k_0	Propagation Constant in Free Space
n_2	Refractive Index of Waveguide
n_1	Refractive Index of Substrate
b	Relative Modal Index
L_0	Transfer Length
s	Waveguide Separation
t	Waveguide Width
λ_0	Wavelength in Free Space
ADC	Analog-to-Digital Converter
BPM	Beam Propagation Method
RDB	Reversed Delta Beta
YPD	Y-Junction Power Divider
ILG	In-Line Gain

ACKNOWLEDGEMENT

Completing this thesis, hence my MSEE, is analogous to reaching the peak of Mt. Whitney in Southern California. Many people attempt and succeed in cresting the peak, but that doesn't diminish the importance of the task to the individual. Although usually clearly marked, the path is still long, laborious, and has many latent obstacles. The final stretch is the toughest.

The NPS facilities, helpful professors, and supportive friends filled my backpack to overflowing. Without any of these the road would have been much tougher. I thank Professor Pieper for introducing me to the interesting world of Photonics and Professor Powers for his objective critique of and valuable comments for this thesis. Friends Bill Ringer and Marty Welch were always there when I needed something. Professor Pace's guidance, support, and vision kept me focused on completing this important personal and professional goal. His best, and I believe most important, trait was his steadfast encouragement and positive outlook. Thank you all.

My lifeline has been my wife, Deborah. She has been consistent with her love, patience, and understanding throughout our brief stay. Although she wasn't up late studying with me or taking tests alongside me, it would have been impossible to achieve this goal without her support. I can never repay her for the gracious gift she has provided. All I can do is acknowledge her gift and thank her. I love you darling. Let's go home.

I. INTRODUCTION

A. BACKGROUND

Analog-to-digital converters (ADCs) are basic building blocks for a wide variety of digital systems. A partial list of ADC applications includes process control, automatic test equipment, video signal acquisition, audio recording for compact discs, and interfaces for personal computers. One approach, known as sigma-delta modulation, employs integration and feedback in iterative loops to obtain high resolution analog-to-digital conversion with single-bit code words.

The integration consists of accumulating the error between the sampled input signal and the discrete feedback signal. Once the magnitude of the accumulated error exceeds a comparator threshold voltage, the output is quantized, fed back, and subtracted from the input. This quantized feedback signal forces the average value of the quantized output to track the average of the input signal. This happens continuously, eventually resulting in an accurate, but time delayed, digital representation of the input signal.

This thesis describes a technique for accumulating optical intensity using fiber lattice structures. Fiber lattice structures incorporating single mode fibers, optical amplifiers, and directional couplers are used to construct these accumulators. Either the directional couplers or the optical amplifier in the feedback can be manipulated to change the accumulation direction. Although much effort is expended describing the intricacies of directional couplers, accumulation direction in this thesis was achieved by varying the optical gain in the feedback of the fiber lattice structure. The extension to manipulating the directional couplers to perform the same function is straightforward, but more tedious.

One of the fiber lattice structures is inserted into an optical implementation of the sigma-delta modulator and the results are compared with known results. Although the first-order results are consistent with the predicted results, the quantization noise is highly correlated to the input. This results in excessive limit cycles. The second-order sigma-delta modulator not only reduces the limit cycles, but also increases the reliability.

B. PRINCIPLE CONTRIBUTIONS

Sigma-delta modulators have been documented and studied extensively [Ref. 2]. The work documented in Reference 2 is primarily electrical in nature. The optical implementation of the sigma-delta modulator described herein was initially described by Ying [Ref. 3]. The accumulators included in the optical sigma-delta modulators were ideal transfer functions for specific coupling ratios. This thesis develops software fiber lattice models with MATLAB Simulink that use voltage-controlled directional couplers and optical amplifiers to perform the accumulation. Results of testing of these models, both independently and included in place of the ideal accumulator transfer functions in the modulators, are also included. The theory behind directional coupling is also described in detail. This thesis also builds the index of refraction of an integrated optical directional coupler that is analyzed with a validated beam propagation method (BPM) program. The BPM-generated plots reinforce the theory and conclusions discussed in the optical switching part of the thesis.

C. THESIS OUTLINE

Optical switching is discussed in Chapter II. Integrated optical directional couplers are used to transfer energy from one waveguide to another. Controlling the energy transfer is the key to rapid or slow accumulation. The theoretical background behind single and split electrode directional couplers is discussed before a beam propagation method program is used to illustrate graphically the transfer of energy in an integrated optical directional coupler.

Chapter III discusses the fiber lattice accumulators. Two models are developed, tested, and compared. The development of the models progresses from the generation of the transfer functions through the testing to conclusions about the operation and dependencies of both models.

In Chapter IV one of the models is inserted into the first-order optical sigma-delta modulator and the results are compared to ideal results [Ref. 3]. Two inputs are tested. The first is a ramp from -1 V to $+1$ V; the second is a dc voltage. The second-order architecture with both fiber lattice accumulators included is shown, but no results are

presented. The limitations, conclusions and recommendations for further study are in Chapter V.

II. OPTICAL SWITCHING

A. DIRECTIONAL COUPLING

One of the primary components in the optical accumulator is the optical directional coupler. This chapter provides the background necessary to understand how optical energy is switched between waveguides, which is the key to accumulating energy. The exchange of power between guided modes of adjacent waveguides is known as directional coupling. The amount of power transferred between adjacent waveguides is dependent on many factors including the propagating modes, waveguide spacing and width, index difference between the substrate and waveguide, and wavelength. These parameters together describe the guiding strength, the propensity of the energy in one waveguide to transfer completely to an adjacent waveguide, in the form of a coupling coefficient, κ, defined as [Ref. 4]

$$\kappa = \frac{2h^2 p e^{-ps}}{\beta(t + \frac{2}{p})(h^2 + p^2)} \tag{1}$$

where

s = waveguide separation,
t = waveguide width,
$\beta = k_0 N$, where N is the effective index,
$k_0 = 2\pi/\lambda_0$, the free space propagation constant,
$h = (n_2^2 k_0^2 - \beta^2)^{1/2}$, where n_2 is the index of refraction of the waveguides, and
$p = (\beta^2 - n_1^2 k_0^2)^{1/2}$, where n_1 is the index of refraction of the substrate.

For symmetric waveguides in a homogeneous substrate $n_2 k_0 > \beta > n_1 k_0$. The effective index approximates the waveguide index for strongly guided modes. Strongly guided modes are essential for optical fiber communication, but could potentially inhibit directional coupling because the substrate carries relatively low energy compared to the waveguide. Directional coupling depends on weakly guided modes for transferring energy from one waveguide to another. Weakly guided modes have a lower effective index than strongly guided modes with the substrate index being the lower limit. However, an effective index equal to the substrate index would result in no coupling at all

because the material would be homogeneous. Similarly, an effective index equal to the waveguide index would result in no coupling because all of the energy would be confined to the higher index waveguide itself. Practical directional couplers have an effective index between the substrate and waveguide indices with the higher index being favored. The dependence of κ on the effective index, N, is shown Figure 1a.

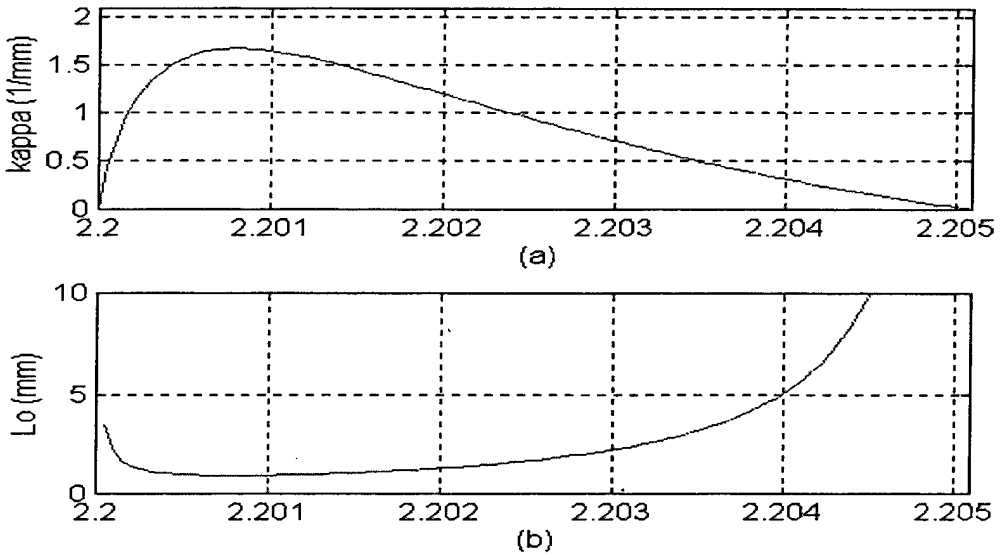

Figure 1: (a) Kappa vs. Effective Index
(b) Transfer Length vs. Effective Index

Figure 1 was generated using Equation 1 with λ_0= 0.9 μm, $s = t = 3$ μm, $n_1 = 2.2$ ($LiNbO_3$) and $n_2 = 2.205$ (Ti indiffusion). Although not practical, N was run from n_1 to n_2. (This was done for illustrative purposes only.) The coupling coefficient is a maximum at $N = 2.2008$. However, as alluded to before, an integrated optical directional coupler N that approximates n_1 will not couple energy; hence this value is not practical. A more realistic value for the parameters used to generate Figure 1a is $N = 2.2034$, which correlates to $\kappa \sim 0.5$ mm^{-1} [Ref. 4]

Another way to determine the guiding strength is to calculate the fiber parameter or V parameter, which is defined as [Ref. 5]

$$V = \frac{2\pi t}{\lambda_0}\sqrt{2 n_1 \delta n} \qquad (2)$$

where

t = waveguide width,
λ_0 = vacuum wavelength,
n_1 = substrate index, and
δn = index difference between waveguide and substrate.

A larger V means stronger guidance and better mode confinement. For the parameters used to generate Figure 1, the V parameter equals 3.14, which correlates to a strongly guided mode. The number of modes the waveguide supports can be found by V modulo π [Ref. 5]. Obviously, this is a single-mode waveguide. Guidance strength can be determined qualitatively by comparing the effective index to the waveguide index (the closer to the waveguide index, the more strongly guided) or quantitatively by calculating the relative modal index, b, defined as [Ref. 6]

$$b = \frac{[(\beta / k) - n_1]}{(n_2 - n_1)} \tag{3}$$

where

$0 < b < 1$,
$\beta / k \equiv N$ = effective index, and
n_2, n_1 = waveguide and substrate index, respectively.

Using the same parameters as those used to generate Figure 1a, the relative modal index equals 0.66, which correlates to a strongly guided mode.

Strongly guided modes will completely couple energy from one waveguide to another, but the modes will have to interact longer. The interaction region is defined as the length of the waveguides when in close proximity to each other [see Figure 2].The transfer length, L_0 [see Figure 1b], is the interaction length necessary to completely

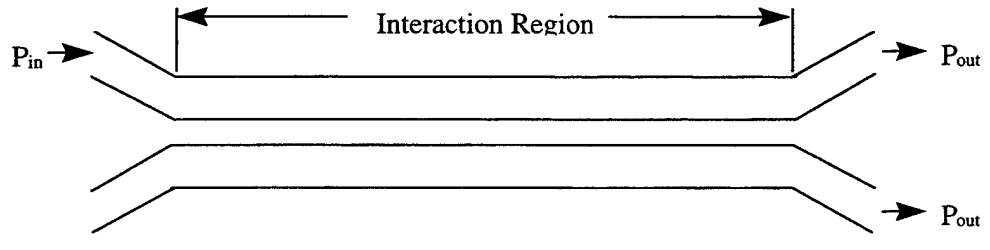

Figure 2: Directional Coupler Interaction Region

transfer the energy from one waveguide to another. For example, if the interaction length in Figure 2 were equal to the transfer length, there would be energy leaving the bottom waveguide only. The transfer length is inversely proportional to the coupling coefficient and is defined as

$$L_0 = \frac{\pi}{2\kappa}. \tag{4}$$

A natural extension of the one-transfer-length-long directional coupler is the 3 dB directional coupler, or 50/50 splitter. A 50/50 splitter is simply a directional coupler with an interaction length equal to $L_0 / 2$. Any coupling ratio can be achieved by fabricating to a specific interaction length and is, in fact, commonplace for passive directional couplers.

The transfer length is used to determine not only the fabrication length, but also the voltage required to drive the directional coupler from one state to another, i.e., from 100% transfer of energy (cross-state) to 0% (bar-state). The dependence on L_0 for two different directional couplers is clarified in the following two sections.

B. SINGLE-ELECTRODE DIRECTIONAL COUPLER

The transfer length for a directional coupler is a common ordinate for directional coupler crossbar plots. In Figure 3, the ordinate values are found by dividing the physical length, L, of the directional coupler by the transfer length, L_0. For example, if $L / L_0 = 3$ the directional coupler is 3 transfer lengths long. The cross symbol at $L / L_0 = 3$ means that the energy will completely transfer three times between the waveguides before arriving at the output port in the adjacent waveguide. To influence the transfer of energy, electrodes are placed on top of the waveguides along the entire length of the interaction region. Once a particular directional coupler is fabricated, a voltage applied to one electrode (the other electrode is grounded) will move the point of operation parallel to the abscissa of Figure 3. The abscissa value is the phase mismatch parameter $\Delta\beta L$ divided by π. The phase mismatch parameter is defined as [Ref. 7]

$$\Delta\beta L = 2\pi\, \delta N\, L / \lambda_0 \tag{5}$$

where

δN = difference between indices, and
λ_0 = vacuum wavelength.

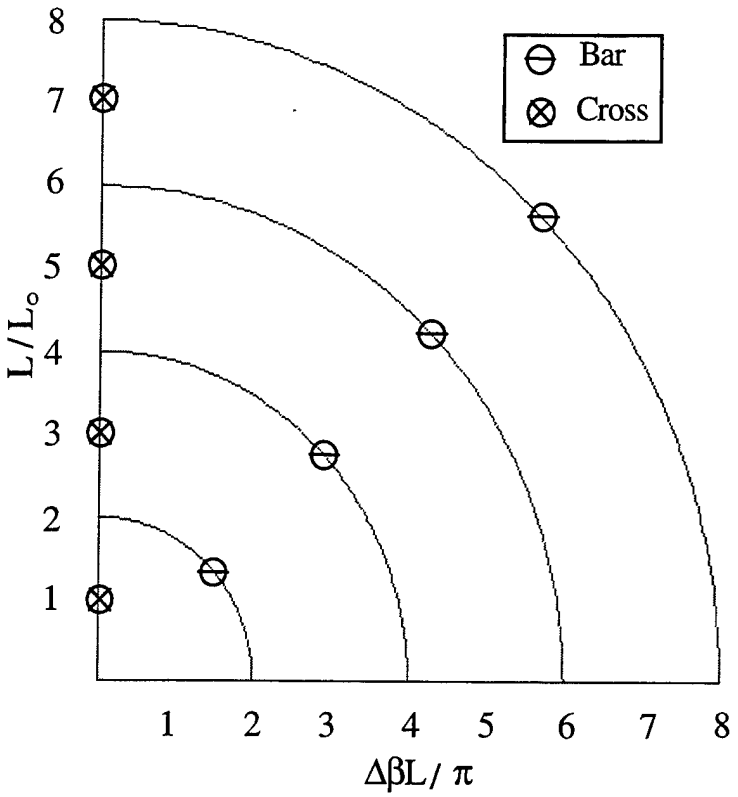

Figure 3: Single Electrode Directional Coupler Crossbar Plot

The difference in the index is due to the electro-optic effect. The electro-optic effect is the change in the refractive index due to the application of a dc or low-frequency electric field. There are two forms of the electro-optic effect. The Pockels effect is linear in nature and is proportional to the applied electric field. The Kerr effect is quadratic in nature and is proportional to the square of the electric field. Although, the Kerr effect becomes significant at higher intensity levels due to the onset of nonlinearities, it is usually considered insignificant when the Pockels effect is present. The accumulators described in this thesis rely on the linear Pockels effect.

The dependence of the coupled power on $\Delta\beta L$ is the key to making electrically activated directional couplers. With identical waveguides, a voltage applied to one electrode will result in an electric field of V/d in one waveguide and $-V/d$ in the other

waveguide, where d can be approximated as the distance between waveguides. The result is a net refractive index difference of [Ref. 7]

$$2\,\delta N = -n_2^3 \varsigma \left(\frac{V}{d} \right) \qquad (6)$$

where

ς is the Pockels coefficient, and
n_2 is the waveguide index.

The applied electric field is on the order of 10^6 V/m. This can be achieved with 3 V applied across a distance of 3 μm.

As an example, consider a single-electrode directional coupler that is $\sqrt{2}\,L_0$ long. This distance is chosen in order to illuminate the difference between the single and split-electrode directional couplers. As shown in Figure 3, a coupler this long will operate between the cross and bar-states. With 0 V_{dc} applied, the coupler will transfer approximately 40% (~$(\sqrt{2}-1)/(2-1)$) of the energy from one waveguide to the adjacent waveguide in this distance. To drive the coupler from this crosstalk state to a bar-state, a phase mismatch of $\sqrt{2}\,\pi$ is necessary. Notice that the single-electrode directional coupler can only be driven to a bar-state. For $s = 3$ μm, $\lambda_0 = 1$ μm, $n_2 = 2.205$, $\varsigma = 30.9 \times 10^{-12}$ m/V and $\kappa = 0.5$ mm^{-1} the required voltage can be found with a combination of Equations 4, 5, and 6. Applying 1.44 V_{dc} to one electrode will completely prevent the energy from partially transferring to the adjacent waveguide. This means that, when the electrode voltage is flipped between 0 V and 1.44 V_{dc}, the coupling ratio will switch between ~40% and 100%. This transfer characteristic will prove useful when combined with the split- electrode directional coupler, commonly known as the Reversed Delta Beta directional coupler.

C. REVERSED DELTA BETA DIRECTIONAL COUPLER

The two-section Reversed Delta Beta (RDB) directional coupler is identical to the single-electrode directional coupler except that the electrode is split in half and alternating voltages are applied to the electrodes. All references to the RDB directional coupler are for the two-section case; therefore this detail will be suppressed. Instead of

applying a voltage to a one electrode as in the single-electrode case, a voltage is applied to adjacent and alternate electrodes [see Figure 4]. The electrode denoted by V– can be grounded. The effect of alternating voltages is that instead of being restricted to driving

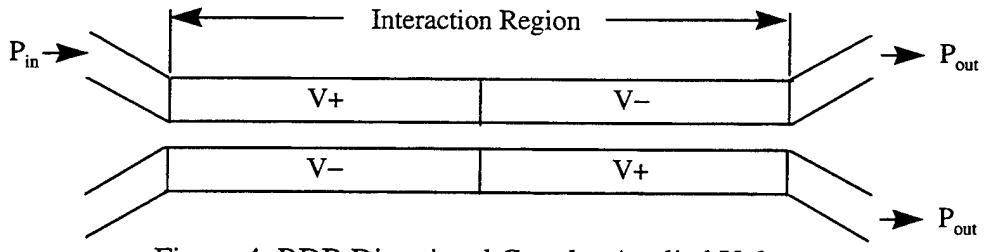

Figure 4: RDB Directional Coupler Applied Voltages

the directional coupler to a bar-state, cross-states can be achieved via voltage adjustment [see Figures 5 and 6]. The main advantage is that the fabrication requirements can be relaxed compared to those required for the single-electrode directional coupler.

The theory discussed in the single-electrode section can be applied to the RDB directional coupler with minor changes. Instead of the electric field inducing a positive change in a waveguide index over the entire interaction length, the particular effect is applicable over half of the interaction length. The negative effect applies over the rest of the interaction length. A single-electrode directional coupler is created when the same voltage is applied to both electrodes on one side of the RDB directional coupler and the opposite electrodes are grounded. Therefore, switching between a particular RDB state and a single-electrode state can be done by simply alternating voltages on either half of the RDB directional coupler [Ref. 8].

An RDB directional coupler $\sqrt{2}\,L_0$ long will exhibit the same characteristics as the single-electrode directional coupler with 0 V applied [see Figures 5 and 6]. However, when a voltage is applied to drive the RDB directional coupler to operate at a different region of the crossbar plot, the first state reached is a cross-state instead of a bar-state. For the same conditions used in the single-electrode example, a voltage of 1.44 V_{dc} applied to alternate electrodes will result in a complete transfer the energy to the opposite waveguide in a distance of $\sqrt{2}\,L_0$. At this distance and voltage the single-electrode

directional coupler was in a bar-state. Increasing the voltage further to reach $\Delta\beta L = 3.74\pi$ will result in a bar-state. Afterwards, only bar-states are achieved with further voltage increases [see Figures 5 and 6]. When used in combination with the single-electrode directional coupler configuration the energy transfer can be controlled by

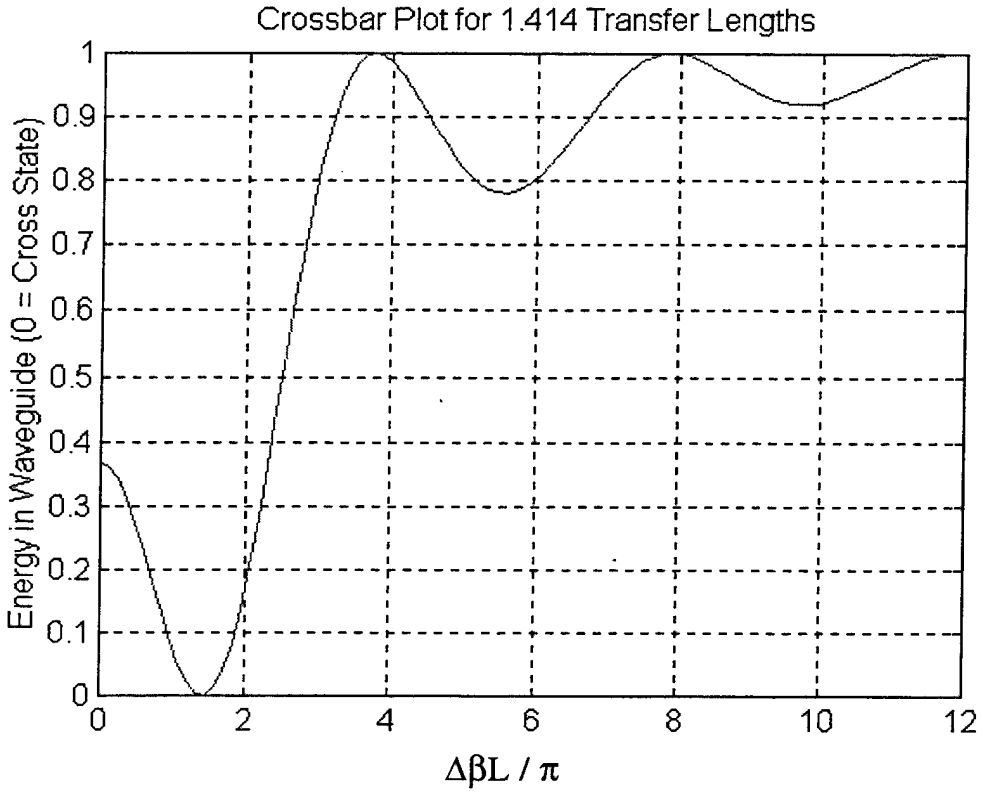

Figure 5: RDB Directional Coupler Transfer Characteristic ($\sqrt{2}\,L_o$ Long)

switching the voltages on one half (the first or second half) of the RDB coupler. When the appropriate voltages are applied in an RDB configuration, energy will completely transfer. Switch the second-half voltages and the energy will exit the directional coupler in the original waveguide. When equal but opposite polarity voltages result in opposite effects, it is known as symmetric switching [Ref. 8]. Similarly, the directional coupler can be driven between any two sets of coupling ratios. This is useful when an input signal is changing rapidly in amplitude or frequency.

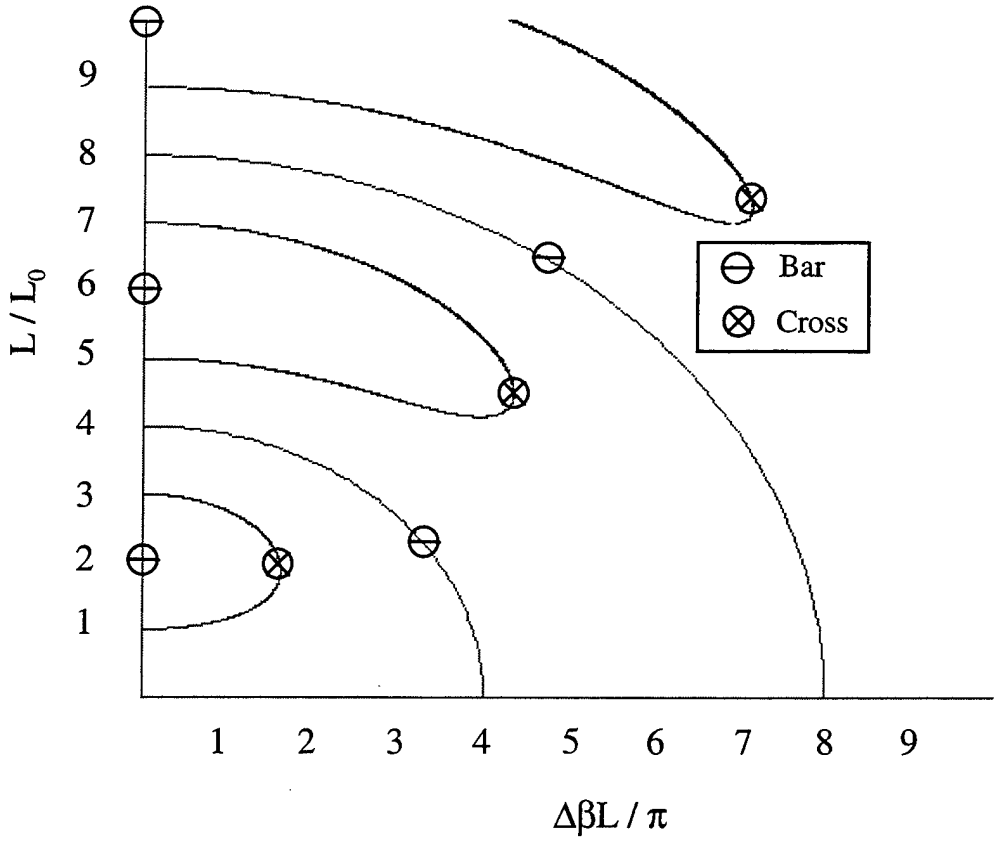

Figure 6: RDB Directional Coupler Crossbar Plot

D. BEAM PROPAGATION METHOD

The Beam Propagation Method (BPM) is a numerical solution to the Helmholtz wave equation that effectively models an optical structure as a series of infinitely thin lenses separated by an incremental axial distance. The BPM consists of a set of Fourier transforms interspersed with complex multiplications in the spatial domain in an iterative algorithm that advances the solution in successive steps along the optic axis [Ref. 9]. An existing program was modified to enable a directional coupler to be modeled. The code used to generate the index itself is located in Appendix A. The output of the index part of the code is shown in Figure 7.

A guided mode is launched into the Y-junction power divider (YPD) and the energy is split between the diverging arms. The arms diverge in order to prevent

inadvertent coupling, or crosstalk, between the modes in each arm. The arms diverge from and converge toward each other at a one degree angle. The waveguide width and separation are both approximately 3 μm.

In order to demonstrate the mode coupling, one arm of the YPD was removed and a symmetric mode was launched into the index. (In Figure 7, this is the bottom arm, in Figure 8 this is the right arm.) Since the guided mode was not adjusted to be centered on the remaining arm of the YPD, a significant part of the energy is initially incident on a substrate index instead of the expected waveguide index. This shock results in a radiation

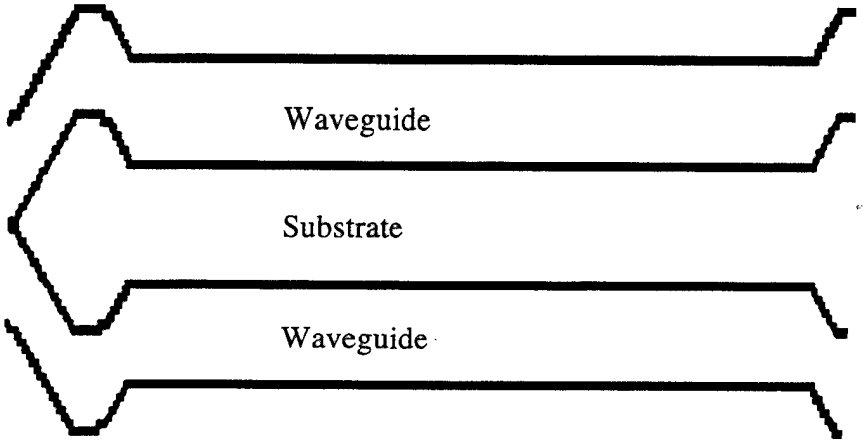

Figure 7: BPM Generated Index

condition shown by the yellow areas among the red substrate in Figure 8. Most of the energy is still inserted into the remaining waveguide as is evident by the pink area in the left arm of the YPD. The energy continues down the arms and enters the interaction region, where the energy begins to immediately transfer to the adjacent waveguide. This is due to the guiding strength described by the coupling coefficient, κ. As the mode continues traveling down the interaction region, energy is continuously transferred until all of the energy resides in the adjacent waveguide. This can be clearly seen by the purple region in the right waveguide. Immediately after completely transferring to the adjacent waveguide the process starts again in reverse. This complete coupling is repeated every transfer length, L_0.

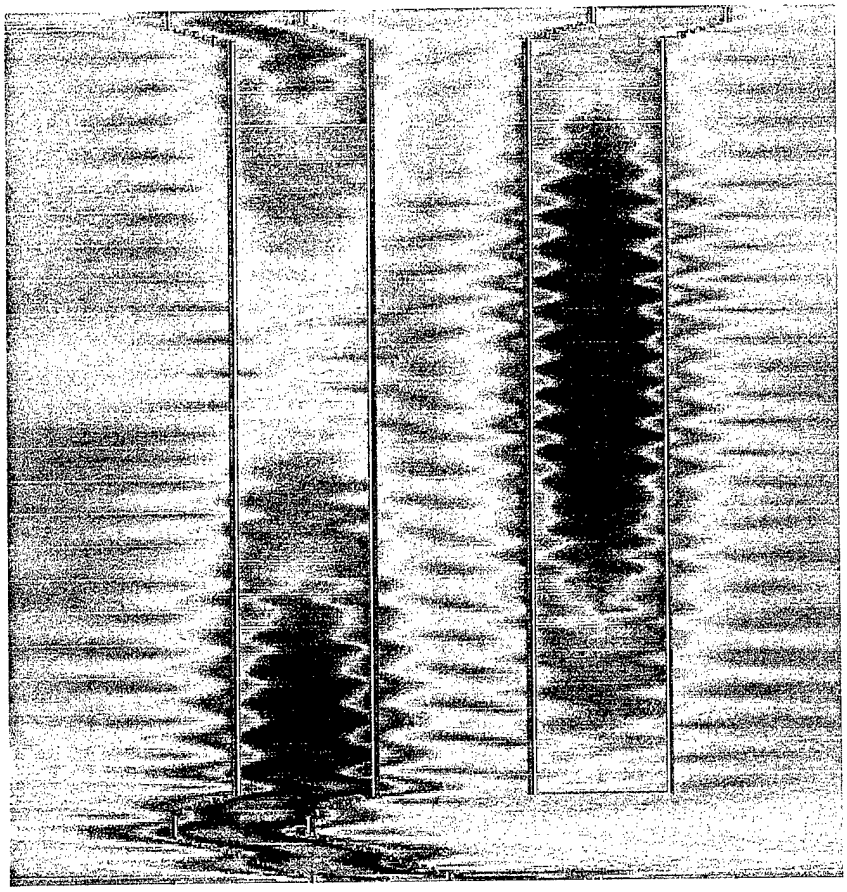

Figure 8: BPM Directional Coupler Operation

If energy were inserted into both waveguides, the interaction would occur simultaneously and continuously. After interacting for one transfer length, the energy resident in either waveguide at the beginning of the interaction region is transferred to the adjacent waveguide. For the directional coupler fed by a YPD as shown in Figure 7, this is neither interesting nor practical. However, the directional couplers described in this thesis have energy incident from two different sources. The input signal is inserted into one waveguide, while a feedback signal is inserted into the adjacent waveguide. The feedback signal originates from the output of a second directional coupler up-line and is

amplified by an optical amplifier before returning to the first directional coupler. The result is that the feedback signal can be greater than the input signal. A carefully chosen coupling ratio can result in combining the energy contained in the two waveguides in any ratio desired, as long as the sum of the cross ratio and the bar ratio equals 1 (disregarding losses). This is the concept behind rapid or slow accumulation. Coupling ratios determine the amount of energy crossed into the feedback loop and, hence, amplified.

Now that the fundamentals have been discussed and demonstrated, the important role of directional couplers can be understood better. The fiber lattice structures discussed next use the directional couplers to accumulate, dump, or combine energy, depending on the requirements. Without the switching capability of directional couplers this would still be possible, but the implementation would incur more losses.

E. SUMMARY

This chapter discussed the theory behind directional coupling. Optical energy incident on one waveguide of a directional coupler will have a tendency to transfer, or enter cross-state, to the adjacent waveguide in a distance known as a transfer length. This transfer distance can be influenced by introducing an electric field across the electrodes on top of the waveguides. The result is that energy can be transferred in any percentage desired according to the crossbar plots. The amount of energy transferred is a critical characteristic in determining fiber lattice structure accumulation rates discussed in Chapter III.

III. FIBER LATTICE STRUCTURES

A. TRANSFER FUNCTIONS

Fiber optic signal processing devices can be constructed to perform various functions, including convolution, correlation, matrix operations, frequency filtering, pulse train generation, and matched filtering. Fiber lattice structures described and used in this thesis depend on the time-domain matrix multiplication capability. A fiber lattice structure can be constructed with a pair of voltage-controlled directional couplers, and intra-coupler single mode-optical fiber lengths. An optical amplifier is added in the feedback to enable accumulation.

The general form of the fiber lattice structure [Ref. 1] is shown in Figure 9. The inputs are X_1 and X_2; the outputs are Y_1 and Y_2. The blocks a_1 and a_0 are the voltage-

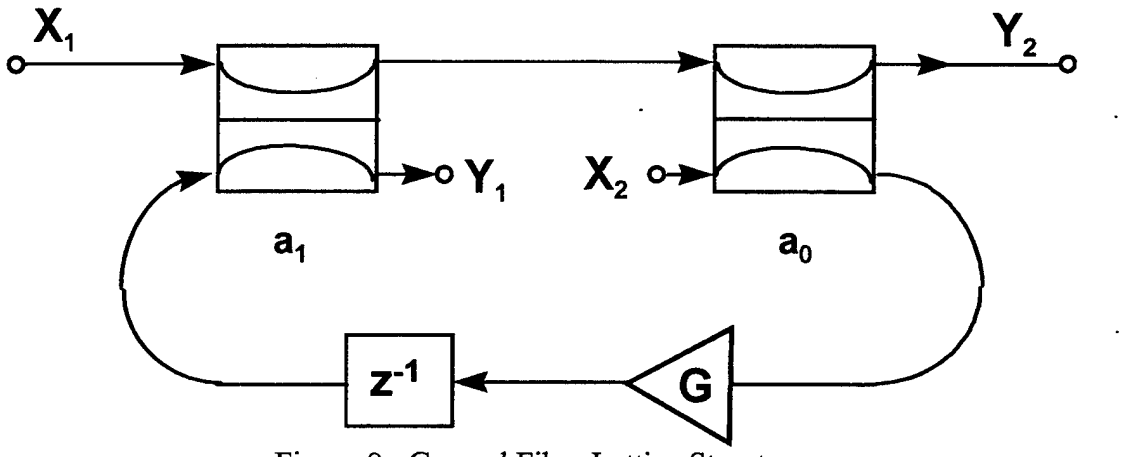

Figure 9: General Fiber Lattice Structure

controlled directional couplers discussed in Chapter II. The lines connecting the input and output to the directional couplers are optical fiber lengths. The gain block G represents an optical amplifier. A feedback delay is represented by the z^{-1} block. Although both X_1 and X_2 are inputs, they are not used simultaneously. Likewise, only one output is used for a particular input. The transfer functions from either input port to either output port are known. The transfer functions of interest here are those from input X_1 to output Y_2 and from input X_2 to output Y_1.

The transfer function from X_1 to Y_2 is designated $H_{21}(z)$. The specific fiber lattice structure for $H_{21}(z)$ is shown in Figure 10. The input signal, X_1, is inserted into A of directional coupler a_1. The energy entering the directional coupler either couples to the

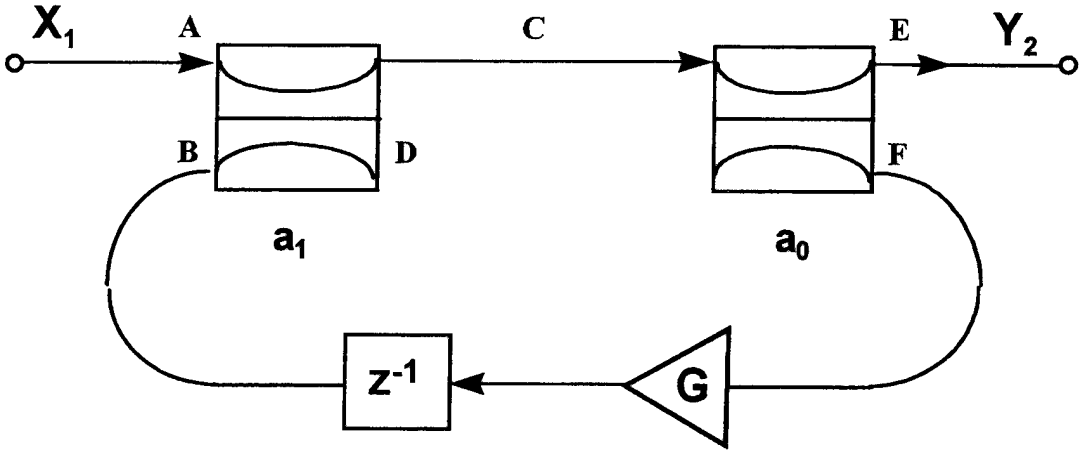

Figure 10: $H_{21}(z)$ Fiber Lattice Structure

adjacent waveguide (D), remains in the original waveguide (C), or combines with the energy from the feedback as determined by the coupling ratio of directional coupler a_1. Energy is inevitably lost to D with the $H_{21}(z)$ fiber lattice structure. An example will illustrate this fact. If a coupling ratio of 0 (a bar-state) is used in order to avoid any energy from A transferring to D, the same coupling ratio will apply to energy arriving at B. Consequently, all energy at B will transfer to D.

Energy from B (cross-state) and A (bar-state) add coherently before arriving at C. Upon entering C of directional coupler a_0, energy will be divided according to the coupling ratio of that directional coupler. Energy that is in bar-state will arrive at the output (E). Cross-state energy will couple to the adjacent waveguide and arrive at F. This energy will undergo both optical gain and delay. The optical gain is performed with either a doped fiber with an optical pump or a semiconductor laser amplifier. The delay is dependent on the period of the pulsed laser used for sampling. A one-period delay was used in the testing section. (As the sampling frequency increases, the length of fiber necessary for a one period delay is shorter.) Finally, this energy returns to B.

Mason's gain rule and block diagram simplification generates the transfer function $H_{21}(z)$ and is depicted in Figure 11. (The input and output are double blocked in this figure.) The $1\text{-}a_1$ and $1\text{-}a_0$ blocks represent the bar-states, while the a_1 and a_0 blocks represent the cross-state or coupling ratio. The energy lost to D is not shown to avoid clutter. The transfer function is

$$H_{21}(z) = \frac{(1-a_0)(1-a_1)}{1-a_0\, a_1\, G\, z^{-1}}. \tag{7}$$

The $H_{21}(z)$ fiber lattice structure is a first-order all-pole system and has one zero at the origin and one pole at $z = a_0 a_1 G$. This fiber lattice structure is stable as long as the pole remains inside the unit circle. This is assured when $a_0 a_1 G < 1$. Since both a_0 and a_1 are ratios and therefore are less than 1, the pole will remain inside the unit circle when $G < 1 / a_0 a_1$. Additionally, the optical amplifier G does not act as an attenuator, therefore $G > 1$. These two limits serve as a check of the results obtained in the testing section. One observation supported later by testing results is that the coupling coefficients are interchangeable.

The transfer function from X_2 to Y_1 is designated $H_{12}(z)$. The specific fiber lattice structure for $H_{12}(z)$ is shown in Figure 12. The input signal is inserted into directional coupler a_0 at A. Cross-state energy is lost to B (similar to that lost to D of Figure 10 by the $H_{21}(z)$ fiber lattice structure). Bar-state energy is summed with cross-state energy from F and arrives at C before undergoing the amplification and delay. Energy arriving at D is divided according to the coupling ratio of directional coupler a_1. Bar-state energy will arrive at the output (E). Cross-state energy will couple to the adjacent waveguide, arrive at F and continue on to directional coupler a_0.

Similar to before, the $H_{12}(z)$ transfer function is generated using Mason's gain rule and block diagram simplification. The result is shown in Figure 13. The energy lost to B is not shown to avoid clutter. The transfer function is

$$H_{12}(z) = \frac{(1-a_0)(1-a_1)\, G\, z^{-1}}{1-a_0\, a_1\, G\, z^{-1}}. \tag{8}$$

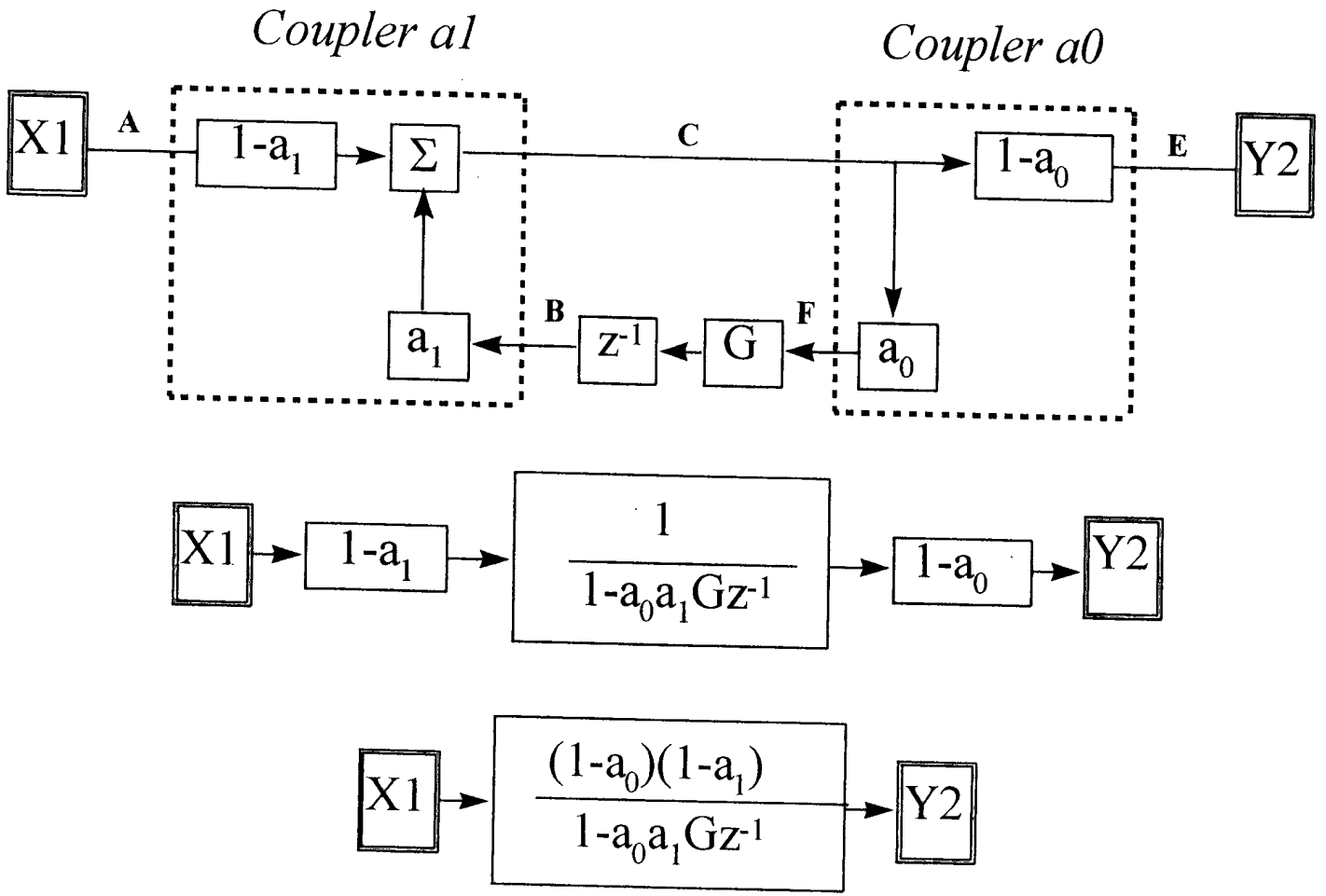

Figure 11: Generation of $H_{21}(z)$ Fiber Lattice Structure

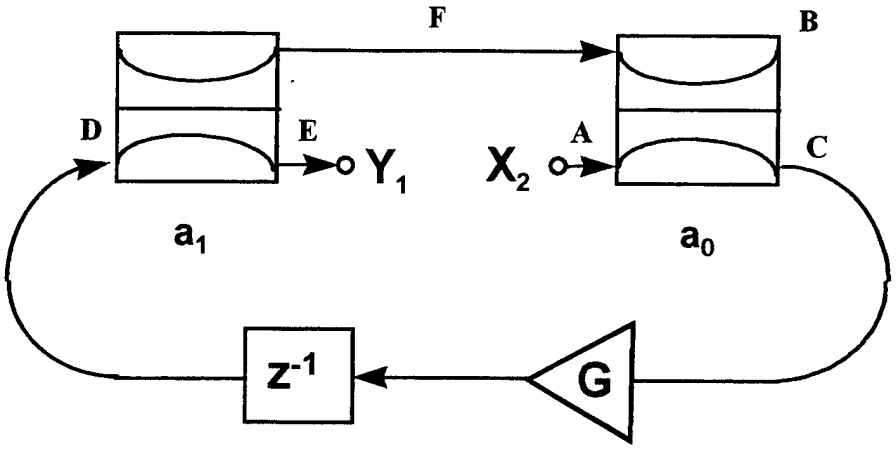

Figure 12: $H_{12}(z)$ Fiber Lattice Structure

The $H_{12}(z)$ fiber lattice structure is a first-order pole-zero system and has the same pole as the $H_{21}(z)$ fiber lattice structure, but has no zeros. Another difference is the optical gain in the feed-forward path. This results in a more rapid accumulation and is discussed further in the testing section. The limitations on the optical gain, hence the pole location, are the same as before and can be summarized as $1 < G < 1 / a_0 a_1$. Again, the coupling coefficients can be interchanged without affecting the transfer function.

B. TESTING OF FIBER LATTICE STRUCTURES

Both fiber lattice models were developed with MATLAB Simulink software. The model for the $H_{21}(z)$ fiber lattice structure is shown in Figure 14. A modified Simulink model of the $H_{12}(z)$ fiber lattice structure is shown later. The directional coupler blocks include the cross and bar-states shown in Figure 11. The X_1 block continually repeats a programmed sequence. For example, a pulse train input is simulated with a constant value repeated at a 1 sample per second rate. The feedback delay block is variable, but was fixed at 1 second for the tests performed.

The first test determines the required optical gain in order for Y_2 to increase monotonically across a range of coupling ratios. If the optical gain is too low, the fiber lattice structure saturates and settles at a fixed value after the typical overshoot and settling associated with damped control systems. If the optical gain is too high, the fiber lattice structure experiences exponential gain because the pole is outside of

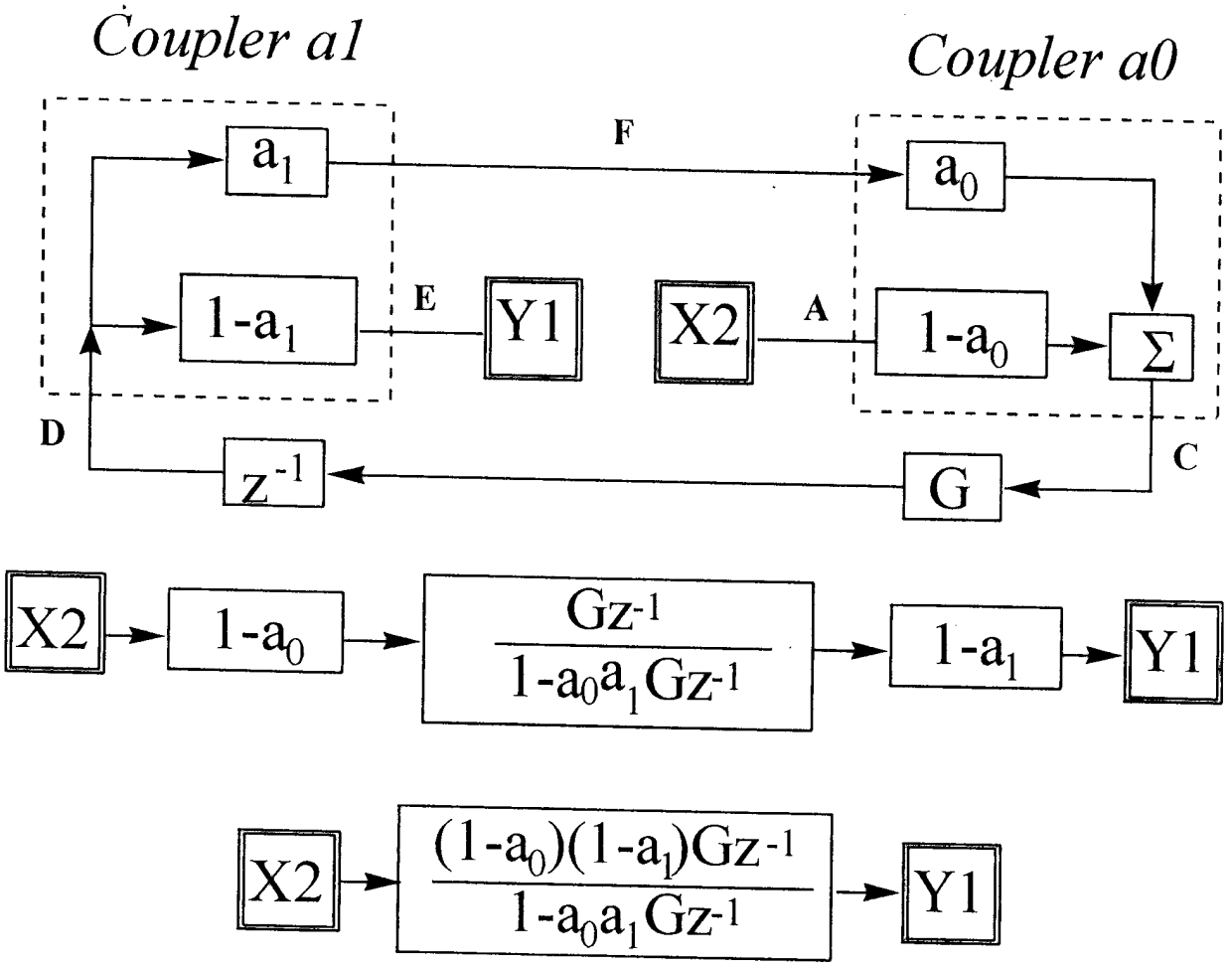

Figure 13: Generation of $H_{12}(z)$ Fiber Lattice Structure

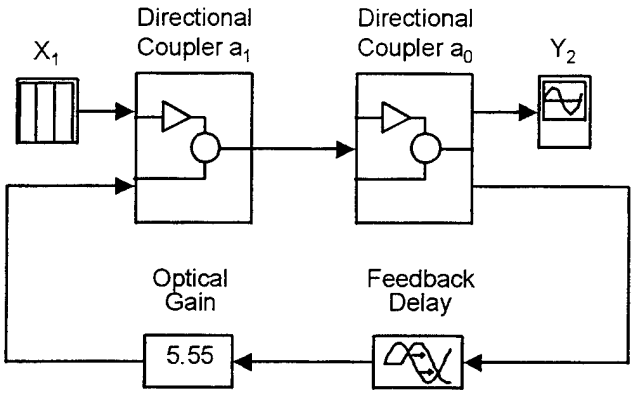

Figure 14: $H_{21}(z)$ Simulink Model

the unit circle. An optical gain that results in a monotonically increasing response is in between these two extremes. An example of all three values of G is shown in Figure 15. In Figure 15, the directional coupler a_1 was programmed for a 0.6 coupling ratio, while directional coupler a_0 had a 0.3 coupling ratio. At these coupling ratios, the G necessary for a monotonically increasing response is 5.555.

The pole location corresponding to this gain and these coupling ratios is $a_0 a_1 G = 1$. Although a pole at z = 1 is stable, an increase in either coupling ratio or in G will quickly result in instability. Conversely, a decrease in either coupling ratio or G will quickly result in saturation and settling. The sensitivity of the $H_{21}(z)$ fiber lattice structure is demonstrated by the small difference in G used in Figure 15 for the exponentially increasing response and the saturated response. The value of G is 5.72 and 5.4 for the exponentially increasing response and a saturated response, respectively. Similarly, the poles for these responses are 1.03 and 0.972, respectively. These characteristics hold for all values of coupling ratios and G when the product $a_0 a_1 G \sim 1$. Table B1 in Appendix B lists the G necessary for a range of a_1 versus a_0 coupling ratios in order to get a monotonically increasing response. This table is a toeplitz matrix. This means that, for a fixed G, the combination of a_0= X and a_1 = Y ($0 < X < 1$ and $0 < Y < 1$)

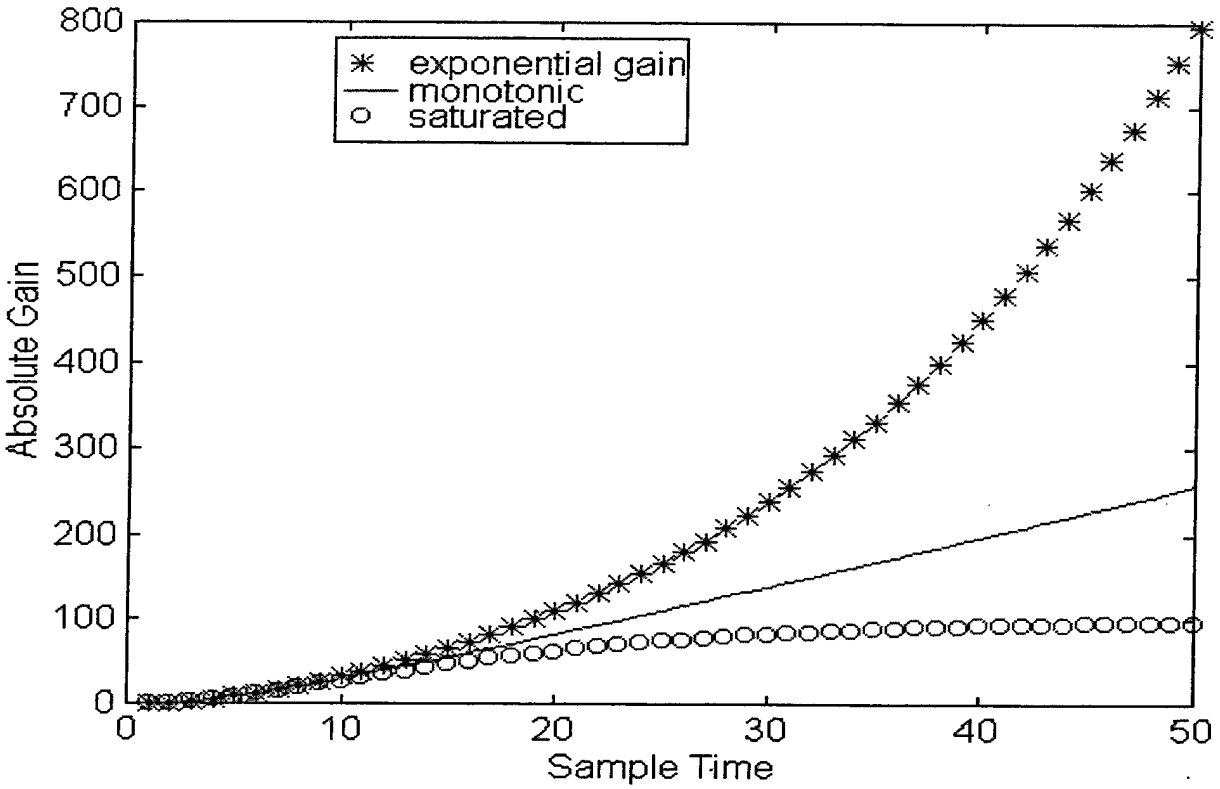

Figure 15: Tuning for Monotonically Increasing Response

results in the same accumulation rates as a_0 = Y and a_1 = X. This fact reinforces the earlier observation that the coupling coefficients in the transfer function are interchangeable. Table B1 and the characteristics discussed above apply to the $H_{12}(z)$ fiber lattice structure too.

Although the optical gain necessary to drive either fiber lattice structure to a monotonically increasing response is the same, the accumulation rate is different. The $H_{12}(z)$ fiber lattice structure accumulates faster because of the optical gain in the feed-forward path. To characterize the accumulation rates of each fiber lattice structure, the sample time necessary to reach an absolute gain of 100 was measured. The $H_{12}(z)$ and $H_{21}(z)$ fiber lattice structures testing results are contained in Tables B2 and B3, respectively. Both tables are again toeplitz matrices. Data from Tables B1, B3, and B2 were used to generate Figures 16a, 16b, and 16c, respectively.

As shown in Figure 16, the accumulation rates for both fiber lattice structures decrease as either coupling ratio increases. The reason for this is again related to the pole

located at $a_0\, a_1\, G$. If either a_0 or a_1 increase, there is a proportional decrease in G for this test. Since G is lower each time through the feedback, the energy arriving back at directional coupler a_1 will be proportionally lower. From there, the bar-state energy will go to the output for the $H_{12}(z)$ fiber lattice structure. For the $H_{21}(z)$ fiber lattice structure, the decreased energy enters cross-state while combining with the bar-state input energy. This energy arrives at directional coupler a_0 before entering bar-state to the output. Either way, the energy at the output decreases with a lower G.

At the higher coupling ratios neither fiber lattice structure accumulates rapidly. The reason for the fall-off is that, as the coupling ratio increases, either the energy is permanently lost (i.e., D in Figure 10 or B in Figure 12) or the energy avoids the output (i.e., path CF in Figure 10 or path DF in Figure 12). Conversely, the accumulation rates are highest at the lower coupling ratios. At the lower coupling ratios, less energy is lost at the outset of accumulation (i.e., D in Figure 10 is avoided) and more energy is directed toward the output (i.e., path CE in Figure 10 or DE in Figure 12). However, for the

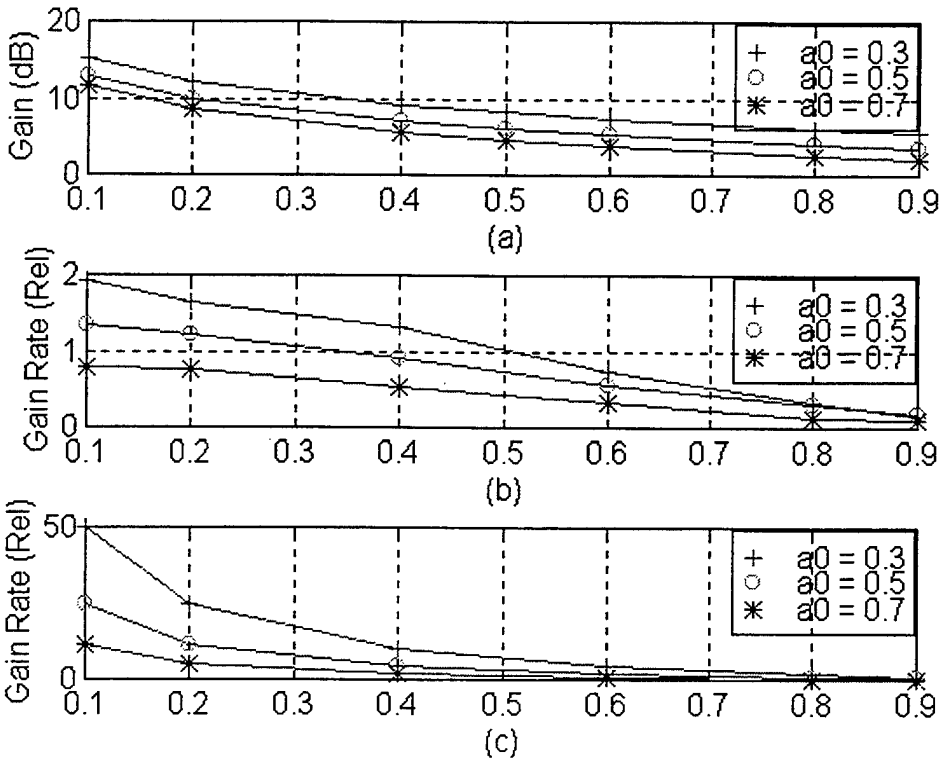

Figure 16: (a) Optical Gain vs a_1 (b) $H_{21}(z)$ Accumulation Rate vs a_1 (c) $H_{12}(z)$ Accumulation Rate vs a_1

$H_{21}(z)$ accumulator a perfect bar-state will experience no accumulation at all because no energy will be crossed into the feedback loop to be increased by the optical amplifier. In fact, the output will be identical to the input.

To show "real-time" results and characteristics of a fiber lattice structure accumulating, the $H_{12}(z)$ fiber lattice structure was modified as shown in Figure 17. It was modified with the addition of a front-end optical amplifier, labeled In-Line Gain (ILG), and a comparator to drive the accumulation up or down. The comparator is modeled by a relay and a switch. When the control signal, simulated by the driver block, is greater than the threshold, the relay latches. The latches cause the switch to flip between the two optical gains. The greater *G*, labeled Accum Up, is for accumulating up and will be selected when driver is greater than the threshold. The other *G* is for accumulating down. The ILG is incorporated now because it is easier to tune the fiber lattice structures without the rest of the circuitry included in the sigma delta modulators in Chapter IV.

The ILG plays a critical role in the $H_{12}(z)$ fiber lattice structure accumulation rate because it is in the feed-forward path. Input X_2 is amplified before any coupling ratio divides the intensity among different ports. The sensitivity of the $H_{12}(z)$ fiber lattice structure to changes in ILG and the accumulation dependence on the comparator signal are shown in Figure 18. The three curves were generated by fixing everything in Figure 17 except the ILG. The coupling ratios used were $a_0 = 0.4$ and $a_1 = 0.5$. The

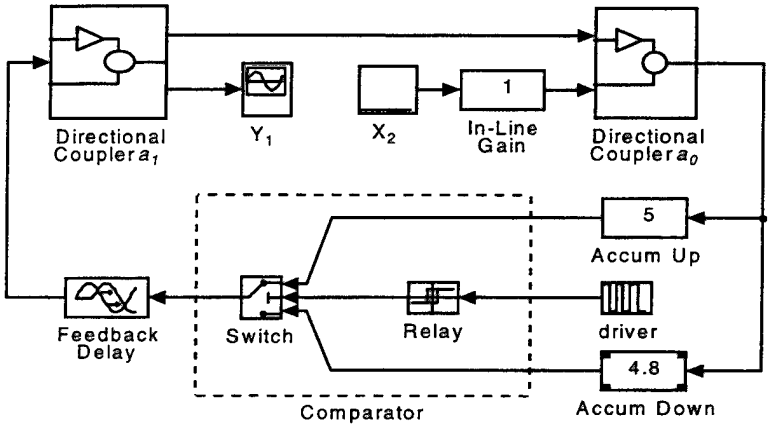

Figure 17: Modified Simulink Model of $H_{12}(z)$ Fiber Lattice Structure

Accum Up *G* used was that for a monotonically increasing response in Table B1. The Accum Down *G* was chosen to generate a smooth curve when accumulating down. Choosing an Accum Down *G* a few tenths less than the Accum Up *G* generally gives good results.

As expected, the accumulation rate is proportional to ILG. This is evident not only in the initial rise from 0, but also in the rise and fall of the oscillating accumulation when the comparator is systematically switching between Accum Up *G* and Accum Down *G*. The relationship between the accumulation direction and the value of the comparator can be seen by comparing the pulses on the bottom of the plot with the peaks and valleys of the oscillations. Also, the value about which the three accumulations oscillate is proportional to ILG. For example, with ILG = 2 the accumulation oscillates about a relative gain of 175. The accumulation with ILG = 3 oscillates at approximately 265, or 3/2 greater than the accumulation with ILG = 2.

When the accumulation first begins, it appears that the first comparator transition from 1 to 0 is ignored because the accumulation continues up. Had Accum Up *G* been set to Accum Down *G* at the onset, the accumulation would have increased to a level above the level achieved when the comparator switched. Consequently, the accumulation continues up. When the second comparator transition occurs, the value is greater than the Accum Down *G* could support; therefore the fiber lattice structure accumulates down as desired. This apparent error is eventually corrected in time.

To show the $H_{12}(z)$ fiber lattice structure dependence on the Accum Down *G*, the ILG was left at 3 and everything else was fixed. A test run with Accum Up $G = 4.8$, instead of 5, results in the fiber lattice structure saturating. Lower values result in a lower saturation value; therefore, the accumulator oscillates at lower values as seen in Figure 19. The Accum Down *G* was set to the Accum Up *G* for reference only. As the Accum *G* decreases, the $H_{12}(z)$ fiber lattice structure settles at a lower value. Although the change in Accum Down drastically affects the magnitude of the steady-state response, the oscillations about the plateau are roughly the same magnitude. One difference between varying the ILG and the Accum Down *G* is that the relative gain rate decreases

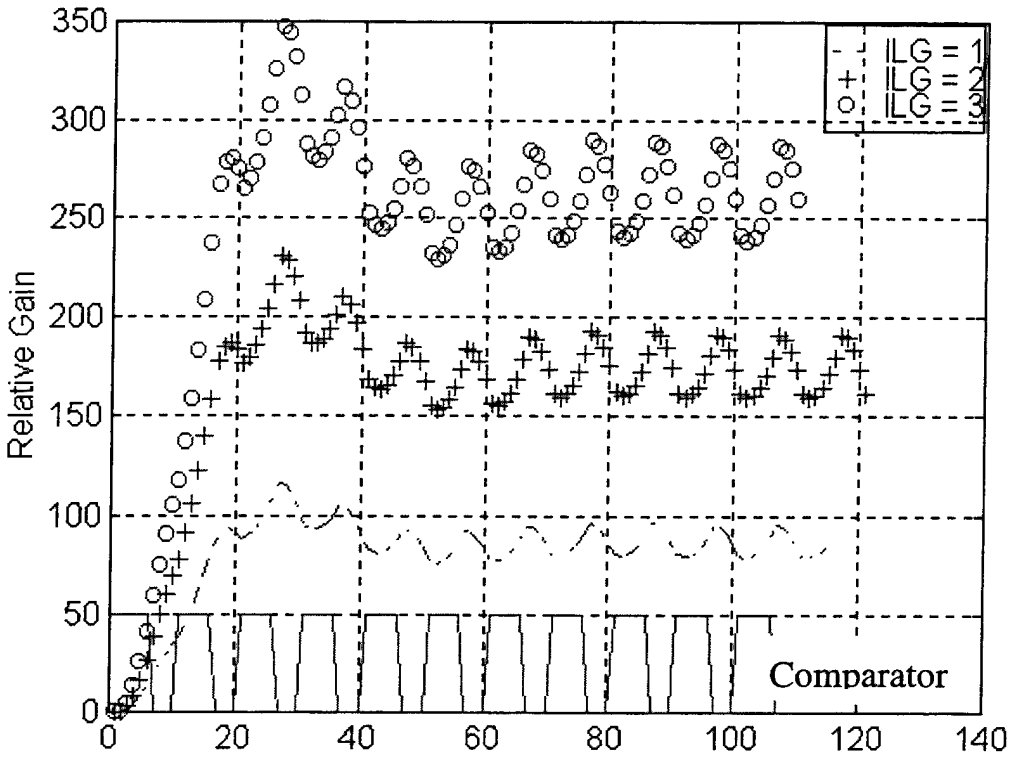

Figure 18: Effect of In-Line Gain on Accumulation Rate

proportionally to the ILG [see Figure 18]. The relative gain rate between peaks and valleys of Figure 19 are approximately the same.

The final test generates the coupling coefficients, ILG, and *G*s required in order for the $H_{12}(z)$ fiber lattice structure to follow a signal. In other words, if X_2 is a step input, Y_1 is the steady state response that settles at the input value. The ILG, Accum Up *G*, and Accum Down *G* versus coupling ratios a_0 and a_1 data are in Tables B4 and B5. To simplify the implementation, the $H_{12}(z)$ fiber lattice structure was tuned with ILG equal to the Accum Up *G*. As mentioned before, good results can be generated with Accum Down *G* a few tenths less than the Accum Up *G*.

In summary, the fiber lattice structures discussed have one distinguishing characteristic and many common characteristics. The lone difference between them is the accumulation rates as shown in Figure 16 and Tables B1, B2, and B3. The $H_{12}(z)$ fiber lattice structure accumulates more rapidly than the $H_{21}(z)$ fiber lattice structure for a

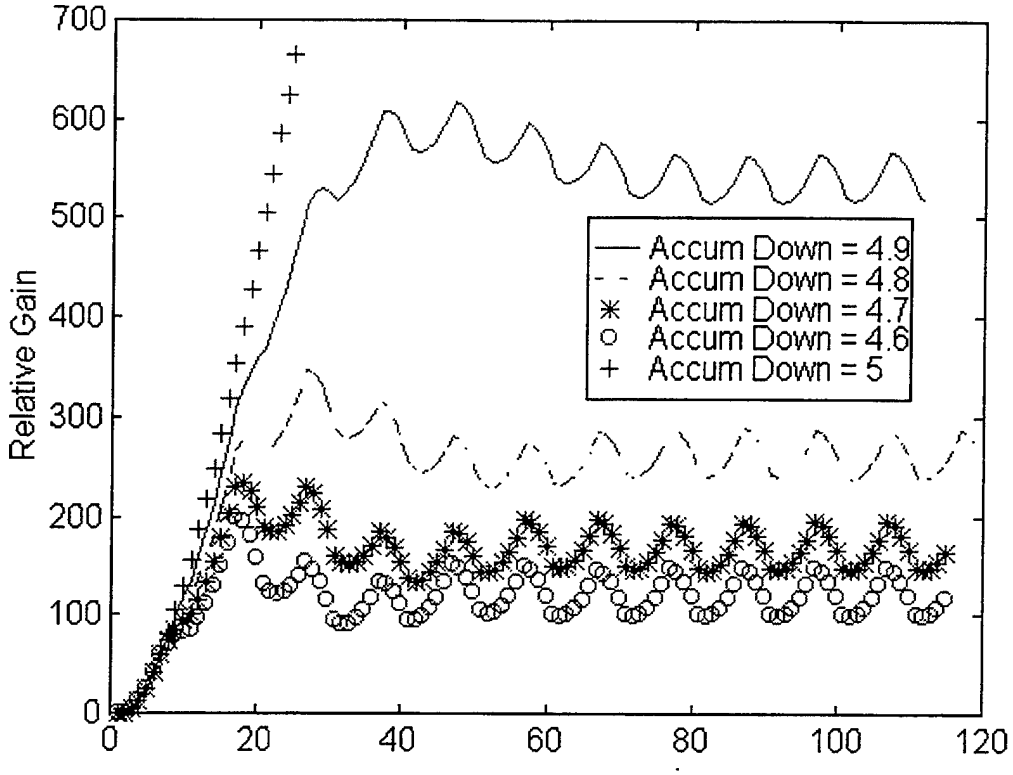

Figure 19: Effect of Reducing Accumulate Down G

given set of coupling ratios and Gs. The type of accumulation can be determined simply by knowing the pole position given by $a_0 a_1 G$. If $a_0 a_1 G < 1$, the fiber lattice structure will saturate; conversely, if $a_0 a_1 G > 1$, the output from the fiber lattice structure will grow exponentially. Monotonically increasing response will occur when the single pole is between the two extremes, which occurs when $a_0 a_1 G = 1$.

The resiliency of the fiber lattice structure is further demonstrated by the fact that the coupling ratios are interchangeable between both directional couplers. This characteristic is shown by the tables in Appendix B. All of the tables are toeplitz matrices. Tracking a signal with varying amplitude or frequency is as simple as controlling the optical gains and/or the voltage-controlled coupling ratios.

C. SUMMARY

Two fiber lattice structures were developed, tuned, characterized, and tested in this chapter. Both fiber lattice structures exhibit similar characteristics with one

exception, the accumulation rates. The $H_{12}(z)$ fiber lattice structure accumulates more rapidly because it has an optical amplifier in the feed-forward path. Some characteristics it shares with the slower $H_{21}(z)$ fiber lattice structure are lower relative accumulation rates at higher coupling ratios, identical optical gain to accumulate monotonically, sensitivity to pole position, and sensitivity to not only the value of the optical amplifier in the feedback path, but also to the difference between the Accum Up *G* and Accum Down *G*.

In Chapter IV, the fiber lattice structures are inserted into the sigma-delta modulators. Although a first-order sigma delta modulator is inherently unstable and unreliable, replacing the ideal transfer function with a fiber lattice structure will serve as a proof of concept for optical accumulation. The $H_{12}(z)$ fiber lattice structure is used because it inherently has a wider range of accumulation rates available. Inserting both fiber lattice structures into the second-order sigma delta modulators results in more reliable and stable output.

IV. SIGMA-DELTA MODULATORS

A. FIRST-ORDER SIGMA-DELTA MODULATOR

The optical implementation of a first-order sigma-delta modulator circuit is shown in Figure 20. The details of the components of this circuit and the interaction between them are contained in Reference 3; therefore, for brevity, they will not be

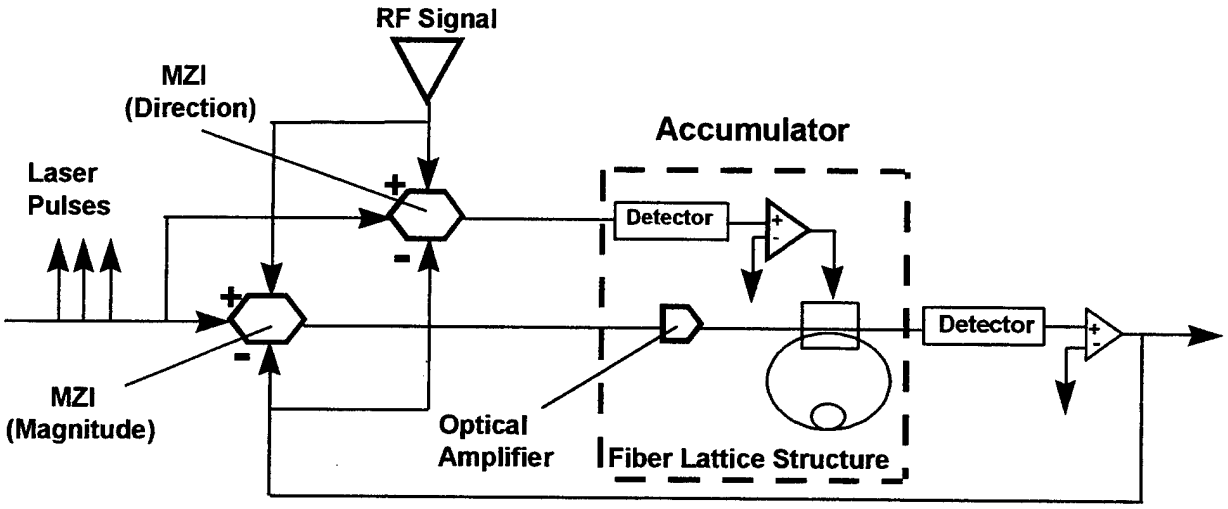

Figure 20: First Order Optical Sigma-delta Modulator

covered here except where necessary. The directional Mach-Zehnder Interferometer (MZI) in Figure 20 was simulated by the driver in Figure 17. The optical output of both the directional MZI here and the driver in Figure 17 are converted to electrical signals by the detectors before becoming the input to the comparator. If the input is greater than the comparator threshold voltage, the fiber lattice structure will accumulate the amplified magnitude MZI energy. Otherwise, the fiber lattice structure will dump energy. As shown in Figure 20, both MZIs receive the same two signals, the input radio frequency (RF) and the discrete feedback from the output comparator. To differentiate between the two MZIs, a different bias is applied. The directional MZI is dc biased with a $-\pi/2$ voltage, while the magnitude MZI is dc biased with a π voltage. The optical amplifier preceding the fiber lattice structure plays the same role as the ILG discussed in Figure 17.

Finally, the laser pulses that are input to both MZIs sample the signal due to the voltage difference between the RF and the discrete feedback signals.

The $H_{12}(z)$ fiber lattice structure inherently has a wider range of accumulation rates; therefore, it is the more appropriate choice for the first-order sigma-delta modulator. Any particular combination of values of coupling ratios, ILG, and G can be pulled from Tables B4 and B5 to demonstrate the validity of the ideal results. The ideal case did not account for either the effect of the optical amplifier in the feed-forward path or the influence of the magnitude MZI. Instead of the magnitude MZI, the normalized directional MZI output was manipulated to closely follow the expected characteristics. The lack of an optical amplifier in the feed-forward path was compensated by an front-end amplifier of 50. Regardless of the these differences, the expected results closely follow those presented here for the same coupling ratios.

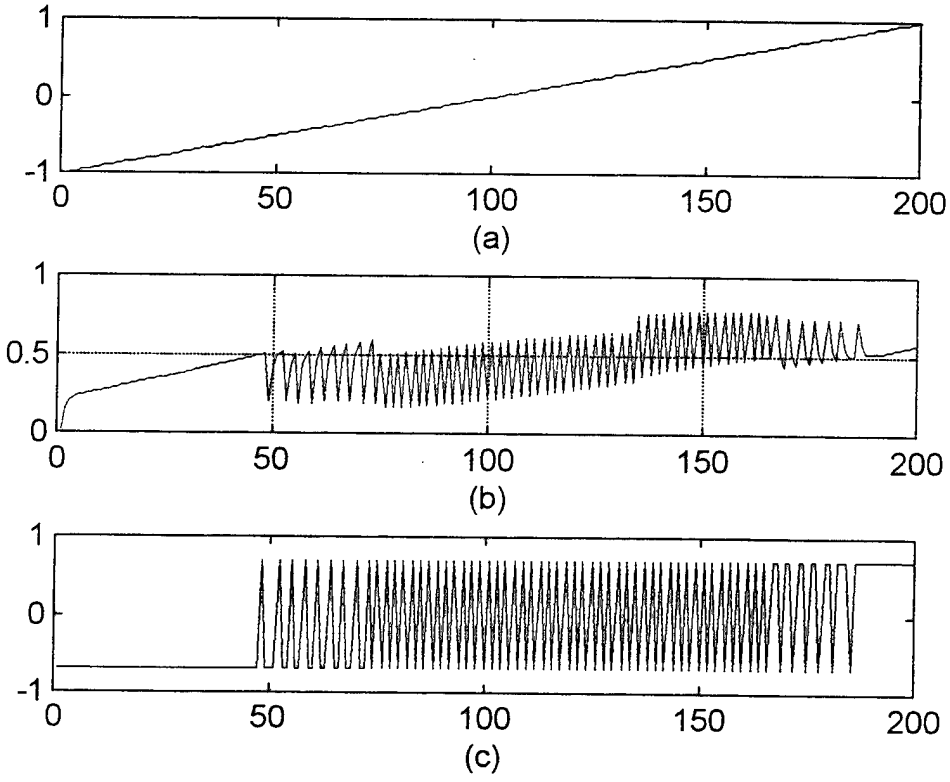

Figure 21: Optical First-Order Sigma-delta (a) Ramp Input
(b) $H_{12}(z)$ Fiber Lattice Structure Output
(c) First-Order Sigma-delta Modulator Output

A ramp signal from –1 V to +1 V is input to both MZIs [see Figure 21a]. The output of the $H_{12}(z)$ fiber lattice structure and the output of the sigma-delta modulator are shown in Figure 21b and c, respectively. These results can be compared to similar results from the ideal case in Figure 22. In part a of both Figures 21 and 22 is the identical ramp input. In Figure 21b, the $H_{12}(z)$ fiber lattice structure accumulates until the comparator threshold of 0.5 V is exceeded. Sometimes there appears to be a lag between penetrating the threshold and the threshold value being subtracted from the MZIs, thereby reducing the $H_{12}(z)$ fiber lattice structure output. This is more a shortfall of the discrete nature of the simulation and the rapid rate of accumulation than a lagging modulator. Once the comparator threshold is breached, the threshold value is subtracted from the next sampled data input at the MZIs before propagating through the modulator

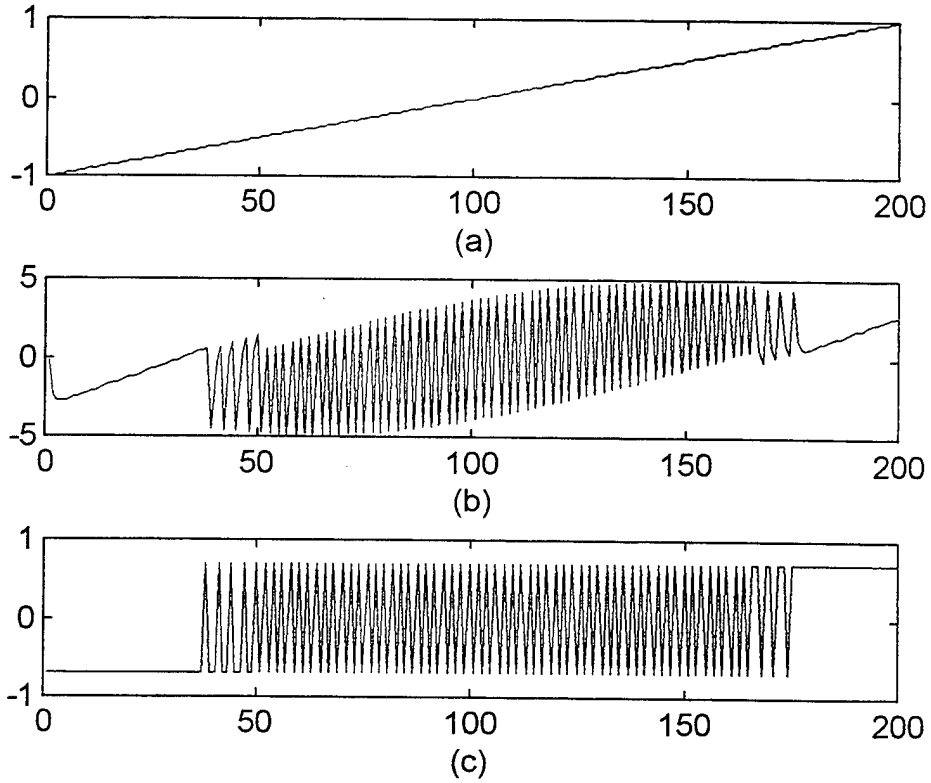

Figure 22: Ideal First-Order Sigma-delta (a) Ramp Input
(b) $H_{12}(z)$ Transfer Function Output
(c) First-Order Sigma-delta Modulator Output

again. The accumulation is more rapid between sample times of 70 and 180 than at other times. This is a function of the difference between the input and feedback signals. As the difference approximates the 0 value, the threshold is approached and exceeded more often. In Figure 22b, the ideal case, the magnitude of the $H_{12}(z)$ transfer function output is greater than that generated in Figure 21b. This is a direct result of the extreme front-end gain of 50 combined with the lack of accounting for the optical amplifier in the feed-forward path of the $H_{12}(z)$ fiber lattice structure. The patterns are similar due to the dependence on the frequency of threshold crossings not the magnitude between the crossings.

The first-order sigma-delta modulator output shown in Figures 21c and 22c is generated with a quantizer level of 0.7 volts. This means that when the comparator threshold is penetrated, a 0.7 V or a –0.7 V signal is generated. When the signal input to the comparator is between the quantizer values, the value of the output signal can be approximated by the weighting of the output. For example, if the discrete output in a given period is high 10% of the time, the magnitude of the signal being quantized is the lower quantizer level (–0.7 V here) plus 10% of the difference between the values, or 1.4 V. The value of the signal at the end of this period of time is approximately –0.56 V.

The accumulation in Figure 21 is not as symmetric as Figure 22. This is due to the influence of the *G* used for accumulating down, Accum Down *G*, shown in Figure 23. Figure 23b is the same as Figure 21c and is a result of Accum Up *G* and ILG equal to 1.74 and Accum Down *G* equal to 1.5. Figures 23a-d were generated by fixing everything except the Accum Down *G*. As the Accum Down *G* decreases, the accumulation rate slows down. This is shown by both the delay before the signal is discretized and the weighting of the discrete signal. As the Accum Down *G* decreases, the signal is not tracked as accurately. For instance, in Figure 23d when the input signal is equal to 1, which occurs at the 200th sample, the discrete output is idling about 0. This corresponds to a value of 0. Conversely, with the other three Accum Down *G*s the discrete output is latched to the resolution of the comparator. This means that the signal

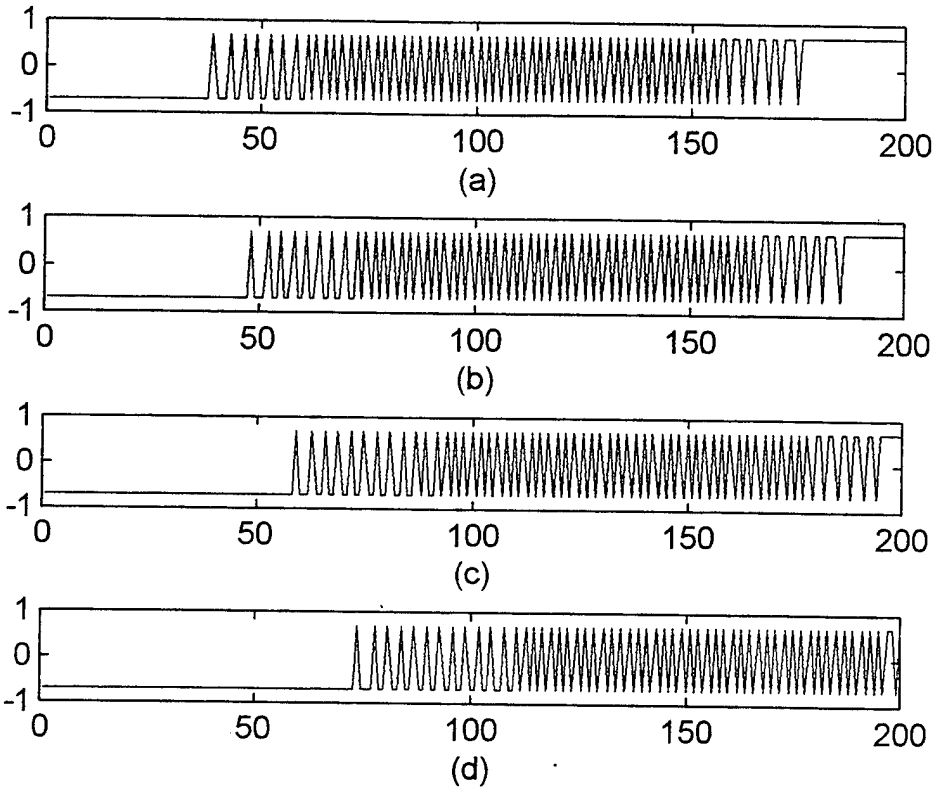

Figure 23: Effect of Accum Down G on First-Order Sigma-delta Modulator Output
(a) Accum Down $G = 1.62$ (b) Accum Down $G = 1.5$
(c) Accum Down $G = 1.38$ (d) Accum Down $G = 1.26$

is at least 0.7 V. Since the input signal is symmetric, it appears that an Accum Down G of 1.62 gives the most accurate results.

Since the accumulation improves as the Accum Down G approaches that of the Accum Up G, it appears that the situation when Accum Down G equals the Accum Up G might generate better results. As shown in Figure 24, the $H_{12}(z)$ fiber lattice structure and the discrete output appear to closely follow the ideal results presented by Ying [Ref. 3] in Figure 22. For a constantly increasing signal like the ramp signal used, removing the Accum Down G seems to be a valid answer. Although that is true, real-world signals vary in frequency and magnitude, thus the need to have two different optical amplifications, Accum Up G and Accum Down G.

Another input signal of interest is a dc signal. An accumulation should result in a discrete output known as pattern noise [Ref. 2]. An input of 0.43 V was inserted in place

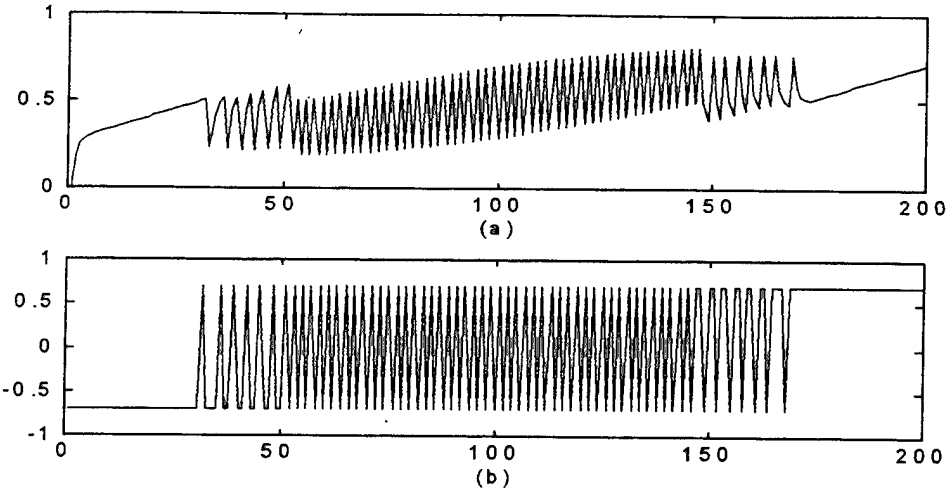

Figure 24: Accumulation with Accum Up Equal Accum Down
(a) $H_{12}(z)$ Output (b) Discrete Output

of the ramp signal used before. The same coupling ratios, Accum Up G, and Accum Down G as used in Figure 21 were used to generate Figure 25. A change in the ILG was necessary because the accumulation rate of the fiber lattice structure was 0.53 for $a_0 = 0.3$ and $a_1 = 0.7$ (see Table B2). The ILG was increased by the inverse of the accumulation rate, thus making it equal to $(0.53)^{-1}$or 3.28.

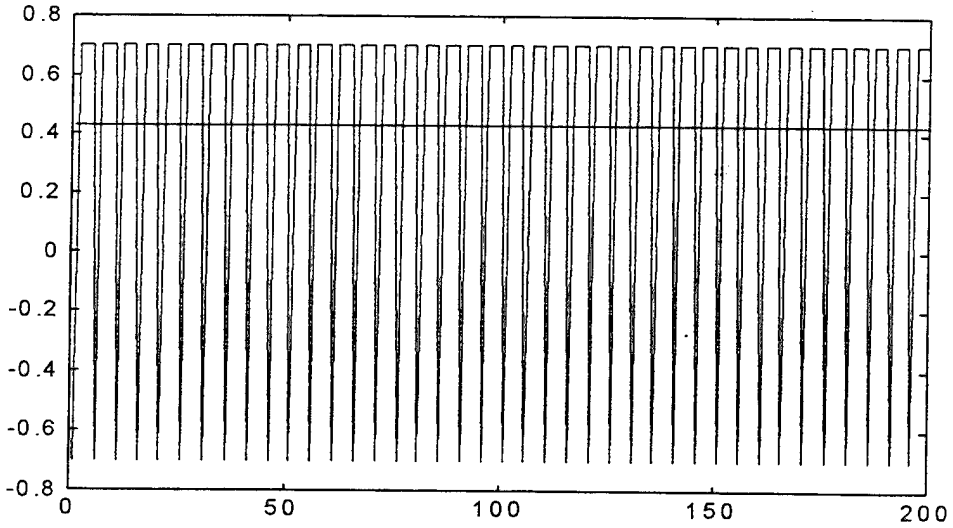

Figure 25: First-Order Sigma-delta Discrete Output with 0.43 V Input

As shown in Figure 25, the discrete output is weighted towards the higher resolution, 0.7 V. The mean of the discrete output is 0.42 which approximately equals the input. The input is shown as a straight line near 0.42.

B. SECOND-ORDER SIGMA-DELTA MODULATOR

The second-order sigma-delta modulator uses both fiber lattice structures discussed in Chapter III. The $H_{21}(z)$ fiber lattice structure is placed in the first stage; the $H_{12}(z)$ fiber lattice structure is inserted into the second stage. Besides this, the difference between the first-order and the second-order is subtle. The optical implementation of the second-order sigma-delta modulator is shown in Figure 26. The first-order output comparator is removed and placed at the output of the second-order modulator. The feedback is compared to a signal in two places, one being the input into the second-order sigma-delta modulator, the other being the output of the first stage. The

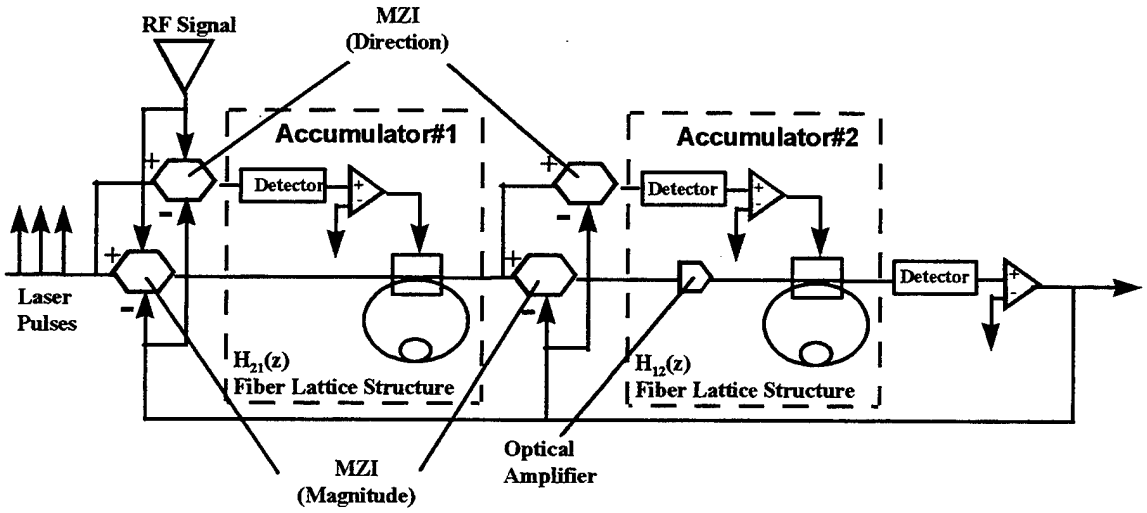

Figure 26: Second-Order Optical Sigma-delta Modulator

combination of the two fiber lattice structures should be a damped and more stable modulator when compared to the first order sigma-delta modulator.

Preliminary results are shown in Figure 27. These results were obtained by setting all coupling coefficients to 0.5, and the front-end gain of the second accumulator to 2. The Accum Up *G* of the $H_{21}(z)$ fiber lattice structure is that for a monotonically

increasing response in Table B3 in Appendix B. For these coupling coefficients this value is 4. The Accum Down *G* was set at a few tenths less at 3.8. For the $H_{12}(z)$ fiber lattice structure the Accum Up *G*, and Accum Down *G* used are found in Tables B4 and B5. The front-end gain was not set to that in the table because the accumulation was too rapid, but to a lower value of 2.

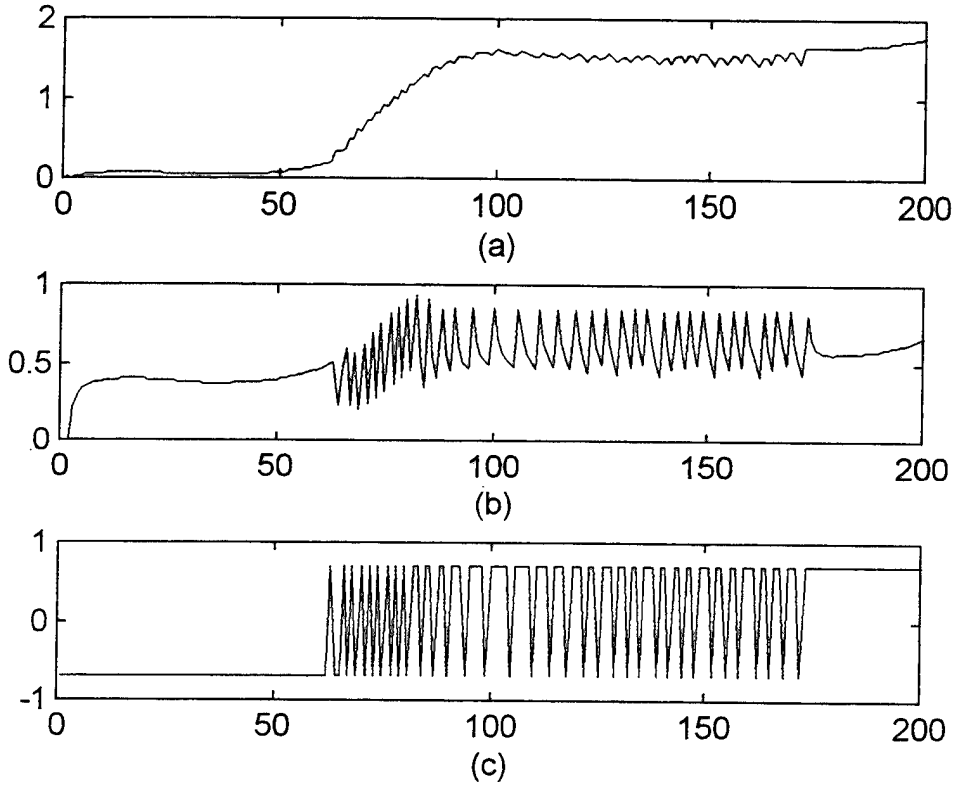

Figure 27: Second-Order Sigma-delta Accumulation (a) $H_{21}(z)$ Output (b) $H_{12}(z)$ Output (c) Modulator Output

The dampling effect of the $H_{21}(z)$ fiber lattice structure on the modulator can be seen in Figure 27a. Once the first stage, $H_{21}(z)$, begins accumulating the second stage, $H_{12}(z)$, follows suit. The second stage and output quickly achieve a 50% duty cycle, meaning every other sample results in an accumulation that penetrates the threshold. The rest of the time oscillations continue with the mean of the idling pattern weighted toward the higher resolution of the output comparator.

Further fine tuning of the second-order sigma-delta modulation is necessary. The accumulation in this example is too rapid, but the outputs shown are symmetrical and convergent. Slower accumulation can be achieved with higher coupling ratios and lower optical gains. This example simply demonstrated that the second-order optical implementation of the second-order sigma-delta modulator is complete and accumulation characteristics are at least comparable to first-order results at this time.

C. SUMMARY

The first-order results presented in this chapter closely resemble the ideal results known a priori. One negligible difference between the ideal and the first-order sigma-delta with the fiber lattice accumulator was in the amplitude of the $H_{12}(z)$ accumulator output. This was due to large front end gain in the ideal case, but proved to be of little concern because the comparator only checks for threshold crossings, not the magnitude reached between crossings.

The lower optical amplifier value, Accum Down *G*, in the feedback determines when accumulation begins. When Accum Down *G* equals Accum Up *G*, the discrete output is symmetrical and looks like an attenuated ideal case. However, this holds only for the particular ramp input signal used. A difference of a few tenths between the Accum Up *G* and Accum Down *G* generally gives good results. A minor change in the optical gain is all that is necessary for the mean of the discrete output to equal a dc input.

Finally, the optical model of the second-order sigma-delta was shown, and preliminary results shown. Further study is necessary to understand how to fine tune the second-order sigma-delta modulator.

V. LIMITATIONS, CONCLUSIONS, AND RECOMMENDATIONS

A. LIMITATIONS

Losses in general were not accounted for in this thesis. This was not because loss is negligible, rather it is a subject more appropriately considered by people better versed at the intricacies involved in implementing an optical device. Integrated optical devices and optical fibers both experience loss. Some losses are insertion, coupling, bend, scattering, radiation, and conversion. Each of these need to be considered before physical construction of either the fiber lattice structures or the sigma delta modulators is attempted.

Directional couplers also experience noise known as crosstalk. Crosstalk occurs when waveguides are in close proximity to each other, similar to coupling in the interaction region. (An example of this can be seen in Figure 8 of Chapter II. After the guided mode exits the interaction region coupling continues to occur when the waveguides are diverging.) Coupling is desirable when controlled, crosstalk results in incomplete states. For instance, theory might predict a bar state, but a practical directional coupler might exhibit a coupling ratio of 0.8. In the BPM modeling of a directional coupler (Chapter II), the splitting angle for the coupler was 0.5 degrees. This angle can not be too extreme because bending losses would occur. However, small angles such as this inherently result in coupling before the waveguides converge at the interaction region [Ref. 9]. Substantial loss or incomplete switching can occur.

Neither the fiber lattice structures nor the sigma delta modulators were tested with an input other than a 1 sample per second ramp or a dc signal. Obviously, more work will be necessary to characterize these devices with more dynamic signals and higher sampling frequencies. The limit on sampling frequency is determined by the length of the feedback. As the frequency increases, the length of the optical fiber decreases proportionally. With a doped fiber optical amplifier, the gain is proportional to length and/or the amount or type of dopant. The higher the dopant index, the slower the energy through the feedback, thus further limiting the sampling frequency. If the length of the feedback delay is kept to the distance that a pulse will propagate in one period, the fiber

lattice structures will be limited to VHF signals at the high end. At the lower sampling frequency the length of the feedback will be dependent on the physical structure where the modulator is located. The bulkiness associated with a long feedback might be overcome by adjusting the directional couplers in the time between pulses to allow energy to recirculate.

The motivation behind using the BPM model was to show the energy coupling back and forth between modes propagating down both waveguides. Directional couplers depend on the odd, or anti-symmetric mode, for complete mode coupling between waveguides. The existing propagation model was only programmed for the symmetric, or even, mode. This limitation resulted in asymmetric and incomplete switching. The steps required for incorporating the anti-symmetric mode are included in Reference 5.

B. CONCLUSIONS

Sigma-delta modulators depend on accumulation of the difference between an input and a feedback signal in order to track the input signal. This thesis develops software fiber lattice models with MATLAB Simulink that use voltage-controlled directional couplers and optical amplifiers to perform accumulation. Both models developed can be easily manipulated to determine the sensitivity of the accumulator to a changing component. The accumulator outputs are consistent with the outputs from the ideal transfer functions shown earlier [Ref. 3].

The fiber lattice structures discussed in this thesis can be easily manipulated to give a wide range of accumulation rates. The characteristics of each accumulator has been discussed and results documented or plotted. Some of the common characteristics are that the coupling ratios are interchangeable, that each accumulator output will increase monotonically for a given set of coupling ratios and a single optical gain, and that the accumulation rates decrease as the coupling ratios increase.

Since both a_0 and a_1 appear together in the transfer function, they can be interchanged without affecting the outcome. Testing results mirrored this observation. All tables in Appendix B are toeplitz matrices. This means that the output for $a_0 = X$ and $a_1 = Y$ will be identical as to the output when $a_0 = Y$ and $a_1 = X$.

The stability of either fiber lattice structure is determined by the pole location. Both fiber lattice structures have the same pole at $z = a_0 a_1 G$. When the product $a_0 a_1 G > 1$, the fiber lattice structure output will grow exponentially. When the product $a_0 a_1 G < 1$, the fiber lattice will saturate and settle at a finite value. When the pole location is at $z = 1$, the accumulator output will be a monotonically increasing response. Both fiber lattice structures are sensitive to changes to pole location.

Although a perfect bar state is possible, no accumulation will occur if both directional couplers in the $H_{21}(z)$ accumulator are adjusted to give a 0 coupling ratio. The reason for this is that the optical amplifier is bypassed; therefore no accumulation occurs. Similarly, if either directional coupler in the $H_{12}(z)$ accumulator is adjusted to be in a cross state, energy is either completely lost or the output is bypassed.

The effect of the optical amplifiers on the accumulation of energy depends on the amplifier location. Both optical amplifiers affect the rate of accumulation and where the accumulators settle. However, the accumulators are much more sensitive to the optical amplifier in the feedback than the front-end amplifier. After settling, the rate of accumulation is directly dependent on the varying gain. For a fixed front-end gain, the accumulation rates after settling depend on the difference between the two optical amplifiers. However, small differences have negligible effect.

The first-order sigma delta modulator with the $H_{12}(z)$ fiber lattice structure inserted closely modeled the ideal results known a priori. Symmetric discrete output results are obtained when the Accum Down G and Accum Up G differ by a few tenths. For a dc input the front-end optical amplifier has to be adjusted by the inverse of the accumulation rate shown in Appendix B for the given coupling ratios. Afterwards, accurate results are obtained.

C. RECOMMENDATIONS

The role of the optical amplifier in the feedback loop is the biggest concern in the design of the accumulators. Further analysis is necessary in order to determine the different options available and the effect on gain. Most research into doped fiber amplifiers is at 1550 nm. Designing with this in mind will help reduce costs.

In this thesis, accumulation direction is accomplished by varying the optical amplifier in the feedback loop of the fiber lattice structures while holding the coupling ratios constant. Accumulation could also be done by varying one or both coupling ratios and holding the optical amplifier at a fixed gain. This would have the same effect because all that matters is the pole location. Varying the coupling ratios would be a bit more tedious, but if a particular change in the coupling ratio can be achieved more precisely than a change in G this would be a better implementation.

Integrating the fiber lattice structures into the second-order sigma delta modulator was attempted with limited success. Certainly with additional fine tuning the accumulation characterstics of the second-order sigma delta modulator will improve and be better understood.

The first-order sigma delta modulator can be implemented with two off-the-shelf fixed-ratio directional couplers and one optical amplifier. This is highly recommended as a proof of concept. A optical modulator offers many advantages over the electrical counterpart, including increased speed and bandwidth.

The switching speed of the integrated optical directional couplers were not discussed in this thesis. This could be a limiting factor in the sampling frequency. This combined with the length of the feedback will determine the maximum sampling frequency. A survey of typical switching speeds should be done in order to quantify this limit.

Finally, the BPM should be updated to include the odd guided mode. This will enable fine design and visualization of any particular integrated optical device. The formulas needed for coding the odd mode can be found in Reference 5.

APPENDIX A: CODE TO GENERATE DIRECTIONAL COUPLER INDEX

This appendix shows the C language code written to create Figures 7 and 8 in Chapter II. It is a modification of existing code used to generate an index of two parallel Mach-Zehnder Interferometers in a substrate. The code shown is part of a larger program named parallel.c.

```
/************************ L 1 ****************************/

                    if(z<(L1)) {


                    a = (int)((W0)/(2.*(DELTAX)));

                    wallleft  = (CENTER) - a;

                    wallright = (CENTER) + a ;

                    for(i=wallleft;i<=wallright;++i)
                        index[i] = (N0) + (DELTAN0);  }

/********************* L 2 P ****************************/

                else if( (z>=(L1)) && (z<((L1)+(L2P))) ) {

                    a = (int)((z-(L1))*tan(ALPHA)/(DELTAX));

                                if(a<1) {a = 1;}


                    b = (int)((W1)/(cos(ALPHA)*(DELTAX)));

                                wallleft  = (CENTER) + a;

                                wallright = wallleft +  b;

                    for(i=wallleft;i<=wallright;++i)
                            index[i] = (N0) + (DELTAN0);

                                wallleft  = (CENTER) - a - b;

                                wallright = (CENTER) - a;

                    for(i=wallleft;i<=wallright;++i)
                        index[i] = (N0) + (DELTAN0);  }


/************************ L 2 ****************************/
```

```
else if( (z>=((L1)+(L2P))) && (z<((L1)+(L2))) ) {

a = (int)((z-(L1))*tan(ALPHA)/(DELTAX));

wallleft  = (CENTER) + a;

wallright = (CENTER) + cross + (int)((W1)/(DELTAX));

for(i=wallleft;i<=wallright;++i)
    index[i] = (N0) + (DELTAN0);

wallleft  = (CENTER)-cross-(int)((W1)/(DELTAX));

wallright = (CENTER) - a;

for(i=wallleft;i<=wallright;++i)
    index[i] = (N0) + (DELTAN0);  }

/******************** L 3 **********************/

else if( ( (z>=((L1)+(L2)) )&&(z<((L1)+(L2)+(L3)) ) ) ) {

b = (int)((W1)/(DELTAX));

wallleft = (CENTER) + cross;

wallright = (CENTER) + cross + b;

for(i=wallleft;i<=wallright;++i)
    index[i] = (N0) + (DELTAN0);

wallleft = (CENTER) - cross - b;

wallright = (CENTER) - cross;

for(i=wallleft;i<=wallright;++i)
    index[i] = (N0) + (DELTAN0);  }

/************************ L 4 P P ********************************/

else if( (z>=((L1)+(L2)+(L3)))

&& z<((L1)+(L2)+(L3)+(L4PP)) )  {

a= (int) ( (z-((L1)+(L2)+(L3)))*tan(ALPHAZ)/(DELTAX) );

if(a<1) {a = 1;}


b = (int)((W1)/(cos(ALPHAZ)*(DELTAX)));

/********* R H S ********/

wallleft = (CENTER) + cross  - a ;
```

```
wallright = wallleft + b   ;

if ( z >= ( ((L1)+(L2)+(L3)+(L4PP))-(int)((W1)/(DELTAX)) ) ) {

for(i=wallleft;i<=wallright;++i)
    index[i] = (N0) + (DELTAN0);  }

else {

wallleft = (CENTER)+cross;

wallright = (CENTER)+cross+(int)((W1)/(DELTAX));

for(i=wallleft;i<=wallright;++i)
    index[i] = (N0) + (DELTAN0);  }

/******** L H S  ***********/

wallright = (CENTER) - cross + a;

wallleft = wallright - b;

if ( z >= ((L1)+(L2)+(L3)+(L4PP))-(int)((W1)*cos(ALPHAZ)/(DELTAX))){

for(i=wallleft;i<=wallright;++i)
    index[i] = (N0) + (DELTAN0);  }

else {

wallright = (CENTER)-cross;

wallleft = (CENTER)-cross-(int)((W1)/((DELTAX)));

for(i=wallleft;i<=wallright;++i)
    index[i] = (N0) + (DELTAN0);  }  }

/****************************** L 4 P ***********************/

else if ( (z>=(((L1)+(L2)+(L3)+(L4PP))))
  &&(z<((L4P)+(L3)+(L2)+(L1))) ) {

a = (int)((z-((L1)+(L2)+(L3)+(L4PP)))*tan(ALPHAZ)/(DELTAX));
    b =(int)((W1)/(cos(ALPHAZ)*(DELTAX)));

wallright  = (CENTER) + cross + (int)((W1)/(2.*(DELTAX)))-  a;
```

```
                wallleft = wallright - b;

                for(i=wallleft;i<=wallright;++i)
                index[i] =(N0) + (DELTAN0);

        wallleft  = (CENTER) - cross- (int)((W1)/(2.*(DELTAX))) + a;
                wallright = wallleft + b;

                for(i=wallleft;i<=wallright;++i)
                index[i] = (N0) +(DELTAN0); }

/************************** L 4 **************************/

else if( (z>=(/*(L4P)+ chg 12/8 atherton*/(L3)+(L2)+(L1)))&&(z<((L4)+(L3)+(L2)+(L1)))) {

        wallright  = (CENTER) + cross +(int)((W1)/(2.*(DELTAX)))+

                zcross + (int)((W1)/(DELTAX));
        wallleft = (CENTER)+cross + (int)((W1)/(2.*(DELTAX))) +((int)((z-
                ((L4PP)+(L3)+(L2)+(L1)))*tan(ALPHAZ)/(DELTAX)));

                for(i=wallleft;i<=wallright;++i)
                index[i] = (N0) +(DELTAN0);

                wallright  = (CENTER) + cross +
                (int)((W1)/(2.*(DELTAX)))-
        ((int)((z-((L4PP)+(L3)+(L2)+(L1)))*tan(ALPHAZ)/(DELTAX)));
          wallleft  = (CENTER) + cross + (int)((W1)/(2.*(DELTAX)))-

                zcross - (int)((W1)/(DELTAX));

        for(i=wallleft;i<=wallright;++i)        index[i] = (N0)
                        + (DELTAN0);

        wallleft = (CENTER) - cross - (int)((W1)/(2.*(DELTAX)))

          -zcross - (int)((W1)/(DELTAX));       wallright =
          (CENTER)-cross-(int)((W1)/(2.*(DELTAX))) -
        ((int)((z-((L4PP)+(L3)+(L2)+(L1)))*tan(ALPHAZ)/(DELTAX)));

        for(i=wallleft;i<=wallright;++i)        index[i] = (N0)
                        + (DELTAN0);

        wallleft = (CENTER) - cross - (int)((W1)/(2.*(DELTAX)))+

        ((int)((z-((L4PP)+(L3)+(L2)+(L1)))*tan(ALPHAZ)/(DELTAX)));
          wallright = (CENTER)-cross-(int)((W1)/(2.*(DELTAX)))

                        +zcross + (int)((W1)/(DELTAX));

                for(i=wallleft;i<=wallright;++i)
                index[i] = (N0)+ (DELTAN0); }

/************************ L 5 ****************************/
```

```
else if( (z>=((L1)+(L2)+(L3)+(L4))) &&
        (z<((L1)+(L2)+(L3)+(L4)+(L5))) ) {

b = (int)((W1)/(DELTAX));

if ( z <= ((L1)+(L2)+(L3)+(L4)+(L5)/2.)) {


wallright = (CENTER) + cross + (int)((W1)/(2.*(DELTAX)))
                                -zcross;

wallleft = wallright - b;

for(i=wallleft;i<=wallright;++i)
index[i] = (N0) + (DELTAN0) + betar; }

else {  wallright = (CENTER) + cross + (int)((W1)/(2.*(DELTAX)))
                                -zcross;

wallleft = wallright - b;


for(i=wallleft;i<=wallright;++i)
index[i] = (N0) + (DELTAN0) + betal; }


if ( z <= ((L1)+(L2)+(L3)+(L4)+(L5)/2.)) {


wallleft = (CENTER) - cross - (int)((W1)/(2.*(DELTAX)))
                                +zcross;

wallright = wallleft + b;

for(i=wallleft;i<=wallright;++i)
index[i] = (N0) + (DELTAN0) + betal; }

else {
wallleft = (CENTER) - cross - (int)((W1)/(2.*(DELTAX)))
                                +zcross;

wallright = wallleft + b;


for(i=wallleft;i<=wallright;++i)
        index[i] = (N0) + (DELTAN0) + betar; } }

/********************** L 6 **********************/

else if( (z>=((L1)+(L2)+(L3)+(L4)+(L5)))        &&
(z<((L1)+(L2)+(L3)+(L4)+(L5)+(L6)-(L6P))) ) {

wallright  = (CENTER)+cross+(int)((W1)/(2.*(DELTAX)))+
```

```
zcross+ (int)((W1)/(DELTAX));

wallleft =(CENTER) +cross + (int)((W1)/(2.*(DELTAX))) +
((int)((((L1)+(L2)+(L3)+(L4)+(L5)+(L6)-(L6PP))-z)*tan(ALPHAZ)/(DELTAX)));

for(i=wallleft;i<=wallright;++i)
index[i] = (N0) + (DELTAN0);

wallright  = (CENTER) + cross + (int)((W1)/(2.*(DELTAX)))-
((int)((((L1)+(L2)+(L3)+(L4)+(L5)+(L6)-(L6PP))-z)*tan(ALPHAZ)/(DELTAX)));

wallleft = (CENTER) + cross +(int)((W1)/(2.*(DELTAX)))-

zcross       - (int)((W1)/(DELTAX));

for(i=wallleft;i<=wallright;++i)
index[i] =(N0) + (DELTAN0);

wallleft = (CENTER) - cross - (int)((W1)/(2.*(DELTAX)))-zcross - (int)((W1)/(DELTAX));

wallright =(CENTER) -cross - (int)((W1)/(2.*(DELTAX)))-((int)((((L1)+(L2)+(L3)+(L4)+(L5)+(L6)-
(L6PP))-z)*tan(ALPHAZ)/(DELTAX)));

for(i=wallleft;i<=wallright;++i)
index[i] =(N0) + (DELTAN0);

wallleft = (CENTER) - cross - (int)((W1)/(2.*(DELTAX)))+
((int)((((L1)+(L2)+(L3)+(L4)+(L5)+(L6)-(L6PP))-z)*tan(ALPHAZ)/(DELTAX)));

wallright = (CENTER) - cross -(int)((W1)/(2.*(DELTAX)))+zcross +

(int)((W1)/(DELTAX));

for(i=wallleft;i<=wallright;++i)
index[i] =(N0) + (DELTAN0);      }

/***************** L 6 P ***************************/

else if( (z>=((L1)+(L2)+(L3)+(L4)+(L5)+(L6)-(L6P))) &&

(z<((L1)+(L2)+(L3)+(L4)+(L5)+(L6)-(L6PP))) ) {

a = (int)((((L1)+(L2)+(L3)+(L4)+(L5)+(L6)-(L6PP))-z)

*tan(ALPHAZ)/(DELTAX));


wallright = (CENTER)+cross+(int)((W1)/(2.*(DELTAX)))-a;
wallleft =  wallright -(int)((W1)/(cos(ALPHAZ)*(DELTAX)));

for(i=wallleft;i<=wallright;++i)        index[i] = (N0) +
(DELTAN0);

wallleft = (CENTER)-cross-(int)((W1)/(2.*(DELTAX)))+a;
```

```
wallright = wallleft + (int)((W1)/(cos(ALPHAZ)*(DELTAX)));

for(i=wallleft;i<=wallright;++i)        index[i] = (N0) +
                                        (DELTAN0);

}

/********************** L 6 P P ********************************/

else if

( z<(((L1)+(L2)+(L3)+(L4)+(L5)+(L6))) ) {

/********* R H S *********/

wallleft = (CENTER)+cross - ((int)((((L1)+(L2)+(L3)+(L4)+(L5)+(L6))-
z)*tan(ALPHAZ)/(DELTAX)));

wallright = (CENTER)+cross+(int)((W1)/(DELTAX)) -
((int)((((L1)+(L2)+(L3)+(L4)+(L5)+(L6))-z)*tan(ALPHAZ)/(DELTAX)));

for(i=wallleft;i<=wallright;++i)                index[i] =(N0) +
                                                (DELTAN0);

/********* L H S ********/

wallright = (CENTER)-cross +
((int)((((L1)+(L2)+(L3)+(L4)+(L5)+(L6))-z)*tan(ALPHAZ)/(DELTAX)));

wallleft = (CENTER)-cross-(int)((W1)/(DELTAX)) +
((int)((((L1)+(L2)+(L3)+(L4)+(L5)+(L6))-z)*tan(ALPHAZ)/(DELTAX)));

for(i=wallleft;i<=wallright;++i)
index[i] =(N0) + (DELTAN0); }

/********************** L 7 ************************/

else {

b = (int)((W1)/(DELTAX));

wallleft = (CENTER) + cross;

wallright = (CENTER) + cross + b;

for(i=wallleft;i<=wallright;++i)
index[i] = (N0) + (DELTAN0);

wallleft = (CENTER) - cross - b;
```

```
        wallright = (CENTER) - cross;

    for(i=wallleft;i<=wallright;++i)
        index[i] = (N0) + (DELTAN0);  }
```

APPENDIX B: FIBER LATTICE TESTING RESULTS

The tables in this appendix contain optical gain values for any particular pair of coupling ratios. Tables B1, B2, and B3 show the values needed for a monotonically increasing response from either accumulator discussed in the text. Tables B4 and B5 show the values needed for accurate first-order sigma delta data conversion.

Coupling Ratio, a_0

Coupling Ratio, a_1	*0.1*	*0.2*	*0.3*	*0.4*	*0.5*	*0.6*	*0.7*	*0.8*	*0.9*
0.1	100	50	33.33	25	20	16.66	14.28	12.5	11.1
0.2	50	25	16.65	12.5	10	8.33	7.15	6.25	5.55
0.3	33.33	16.68	11.11	8.33	6.67	5.55	4.76	4.166	3.703
0.4	25	12.5	8.34	6.25	5	4.166	3.57	3.125	2.78
0.5	20	10	6.68	5	4	3.333	2.85	2.5	2.22
0.6	16.66	8.33	5.55	4.17	3.33	2.78	2.38	2.08	1.85
0.7	14.28	7.14	4.76	3.57	2.86	2.38	2.04	1.785	1.587
0.8	12.5	6.25	4.16	3.125	2.5	2.08	1.785	1.563	1.388
0.9	11.1	5.56	3.7	2.78	2.22	1.852	1.588	1.389	1.234

Table B1: Optical Gain: Monotonically Increasing Response

Coupling Ratio, a_0

Coupling Ratio, a_1	*0.1*	*0.2*	*0.3*	*0.4*	*0.5*	*0.6*	*0.7*	*0.8*	*0.9*
0.1	4.76	3.45	2.70	2.22	1.82	1.49	1.17	0.88	0.54
0.2	3.45	2.38	1.85	1.49	1.20	0.96	0.75	0.54	0.31
0.3	2.70	1.85	1.41	1.11	0.89	0.70	0.53	0.38	0.21
0.4	2.22	1.49	1.12	0.88	0.69	0.54	0.40	0.27	0.12
0.5	1.82	1.20	0.89	0.69	0.54	0.41	0.29	0.20	0.097
0.6	1.47	0.96	0.71	0.54	0.40	0.32	0.21	0.14	0.072
0.7	1.17	0.75	0.53	0.40	0.32	0.21	0.14	0.086	0.036
0.8	0.88	0.54	0.37	0.27	0.20	0.12	0.10	0.07	0.03
0.9	0.53	0.32	0.18	0.16	0.09	0.07	0.036	0.03	0.025

Table B2: $H_{12}(z)$ Accumulation Rate: Monotonically Increasing Response

APPENDIX B: FIBER LATTICE TESTING RESULTS

Coupling Ratio, a_0

Coupling Ratio, a_1	*0.1*	*0.2*	*0.3*	*0.4*	*0.5*	*0.6*	*0.7*	*0.8*	*0.9*
0.1	0.471	0.437	0.397	0.358	0.314	0.270	0.204	0.153	0.079
0.2	0.437	0.403	0.370	0.330	0.289	0.243	0.195	0.138	0.077
0.3	0.397	0.370	0.333	0.298	0.262	0.221	0.175	0.125	0.068
0.4	0.358	0.330	0.298	0.266	0.232	0.196	0.149	0.107	0.059
0.5	0.314	0.289	0.262	0.232	0.201	0.165	0.129	0.091	0.043
0.6	0.270	0.243	0.221	0.196	0.165	0.140	0.108	0.068	0.042
0.7	0.204	0.195	0.175	0.149	0.129	0.108	0.086	0.063	0.031
0.8	0.153	0.138	0.125	0.107	0.091	0.068	0.063	0.051	0.023
0.9	0.079	0.077	0.068	0.059	0.053	0.042	0.031	0.023	0.020

Table B3: $H_{21}(z)$ Accumulation Rate: Monotonically Increasing Response

Coupling Ratio, a_0

Coupling Ratio, a_1	*0.1*	*0.2*	*0.3*	*0.4*	*0.5*	*0.6*	*0.7*	*0.8*	*0.9*
0.1	1.1	1.16	1.235	1.325	1.436	1.587	1.8	2.145	2.873
0.2	1.16	1.22	1.285	1.36	1.462	1.59	1.772	2.05	2.585
0.3	1.235	1.285	1.338	1.407	1.49	1.597	1.74	1.95	2.315
0.4	1.325	1.36	1.407	1.46	1.523	1.603	1.705	1.847	2.067
0.5	1.436	1.462	1.49	1.523	1.562	1.609	1.667	1.742	1.844
0.6	1.587	1.59	1.597	1.603	1.609	1.617	1.626	1.637	1.65
0.7	1.8	1.772	1.74	1.705	1.667	1.626	1.582	1.534	1.483
0.8	2.145	2.05	1.95	1.847	1.742	1.637	1.534	1.434	1.339
0.9	2.873	2.585	2.315	2.067	1.844	1.65	1.483	1.339	1.216

Table B4: $H_{12}(z)$ Optical and In-Line Gain Necessary for Steady State Response

APPENDIX B: FIBER LATTICE TESTING RESULTS

Coupling Ratio, a_0

Coupling Ratio, a_1	*0.1*	*0.2*	*0.3*	*0.4*	*0.5*	*0.6*	*0.7*	*0.8*	*0.9*
0.1	1	1	1.219	1.2	1.3	1.4	1.55	1.85	2.5
0.2	1	1.06	1.2	1.2	1.35	1.4	1.5	1.8	2.3
0.3	1.219	1.2	1.2	1.25	1.35	1.45	1.5	1.8	2.15
0.4	1.2	1.2	1.25	1.3	1.35	1.45	1.5	1.7	1.95
0.5	1.3	1.35	1.35	1.35	1.4	1.5	1.55	1.65	1.78
0.6	1.4	1.4	1.45	1.45	1.5	1.5	1.55	1.57	1.6
0.7	1.55	1.5	1.5	1.5	1.55	1.55	1.5	1.48	1.47
0.8	1.85	1.8	1.8	1.7	1.65	1.57	1.48	1.42	1.33
0.9	2.5	2.3	2.15	1.95	1.78	1.6	1.47	1.33	1.21

Table B5: $H_{12}(z)$ Optical Gain Necessary for Steady Accumulation Down

LIST OF REFERENCES

1. B. Moslehi, J.W. Goodman, M. Tur, and H.J. Shaw, "Fiber-optic lattice signal processing," *Proc. IEEE,* Vol. 72, No. 7, pp. 909-930 1984.

2. J.C. Candy and G.C. Temes, "Oversampling methods for A/D and D/A conversion," in *Oversampling Delta-Sigma Data Converters*, J.C. Candy and G.C. Temes, Eds., pp. 1-29, IEEE Press, New York, NY 1992.

3. S.J. Ying, "Integrated optical sigma-delta modulators," Master's Thesis, Naval Postgraduate School, Monterey, CA, 1981.

4. Yariv, A. and Yeh, Y., *Optical Waves in Crystals*, pp. 459-467, John Wiley & Sons, New York, NY 1984.

5. Z. Weissman, A. Hardy, and E. Marom, "Mode-dependent radiation loss in Y Junctions and Directional Couplers," *IEEE Journal of Quantum Electronics*, Vol. 25, No. 6, pp. 1200-1208, 1989.

6. J.P. Powers, *An Introduction to Fiber Optic Systems*, pp. 20-23, Richard D. Irwin, Chicago, IL, 1993.

7. B.E.A. Saleh and M.C. Teich, *Fundamentals of Photonics*, pp. 707-709, John Wiley & Sons, New York, NY, 1991.

8. A.J. Weierholt, S Neegard, and A.R. Mickelson, "Eigenmode analysis of optical switches in $LiNbO_3$ - theory and experiments," *IEEE Journal of Quantum Electronics*, Vol. 24, No. 12, pp. 2477-2490, 1988.

9. C.C. Foster, "Numerical modeling of opto-electronic integrated circuits," Master's Thesis, Naval Postgraduate School, Monterey, CA, 1994.

10. T.K. Findakly and F.J. Leonberger, "On the crosstalk of reversed $\Delta\beta$ directional coupler switched," *IEEE Journal of Lightwave Technology,* Vol. 6, No. 1, pp. 36-39, 1988.

INITIAL DISTRIBUTION LIST

1.	Defense Technical Information Center 8725 John J. Kingman Rd., STE 0944 Ft. Belvoir, VA 22060-6218	2
2.	Dudley Knox Library Naval Postgraduate School 411 Dyer Rd. Monterey, CA 93943-5101	2
3.	Chairman, Code EC Department of Electrical and Computer Engineering Naval Postgraduate School Monterey, CA 93943-5121	1
4.	Prof. Phillip E. Pace, Code EC/Pc Department of Electrical and Computer Engineering Naval Postgraduate School Monterey, CA 93943-5121	3
5.	Prof. John P. Powers, Code EC/Po Department of Electrical and Computer Engineering Naval Postgraduate School Monterey, CA 93943-5121	1
6.	Mr. Peter K. Burke 412 TW/TSVD 195 E. Popson Edwards AFB, CA 93523	1
7.	Adam F. Atherton 16746 Highfalls Dr. Canyon Country, California 91351	5